sustainability

Article

Integration of Superconducting Magnetic Energy Storage for Fast-Response Storage in a Hybrid Solar PV-Biogas with Pumped-Hydro Energy Storage Power Plant

Takele Ferede Agajie [1,2,*], Armand Fopah-Lele [3,*], Ahmed Ali [4], Isaac Amoussou [1], Baseem Khan [4,5,6], Mahmoud Elsisi [7,8], Wirnkar Basil Nsanyuy [1], Om Prakash Mahela [9], Roberto Marcelo Álvarez [6,10] and Emmanuel Tanyi [1]

1 Department of Electrical and Electronic Engineering, Faculty of Engineering and Technology, University of Buea, Buea P.O. Box 63, Cameroon
2 Department of Electrical and Computer Engineering, Debre Markos University, Debre Markos P.O. Box 269, Ethiopia
3 Department of Mechanical and Industrial Engineering, Faculty of Engineering and Technology, University of Buea, Buea P.O. Box 63, Cameroon
4 Department of Electrical and Electronic Engineering Technology, Faculty of Engineering and the Built Environment, University of Johannesburg, Johannesburg 2006, South Africa
5 Department of Electrical and Computer Engineering, Hawassa University, Hawassa 1530, Ethiopia
6 Department of Project Management, Universidad Internacional Iberoamericana, Campeche 24560, Mexico
7 Department of Electrical Engineering, National Kaohsiung University of Science and Technology, Kaohsiung City 807618, Taiwan
8 Electrical Engineering Department, Faculty of Engineering at Shoubra, Benha University, Cairo 11629, Egypt
9 Power System Planning Division, Rajasthan Rajya Vidyut Prasaran Nigam Limited, Jaipur 302005, India
10 Higher Polytechnic School, Universidad Europea del Atlántico, C/Isabel Torres 21, 39011 Santander, Spain
* Correspondence: tferede19@gmail.com (T.F.A.); a.fopah-lele@ubuea.cm (A.F.-L.)

Citation: Agajie, T.F.; Fopah-Lele, A.; Ali, A.; Amoussou, I.; Khan, B.; Elsisi, M.; Nsanyuy, W.B.; Mahela, O.P.; Álvarez, R.M.; Tanyi, E. Integration of Superconducting Magnetic Energy Storage for Fast-Response Storage in a Hybrid Solar PV-Biogas with Pumped-Hydro Energy Storage Power Plant. *Sustainability* **2023**, *15*, 10736. https://doi.org/10.3390/su151310736

Academic Editor: Gaetano Zizzo

Received: 25 April 2023
Revised: 15 June 2023
Accepted: 3 July 2023
Published: 7 July 2023

Abstract: Electric distribution systems face many issues, such as power outages, high power losses, voltage sags, and low voltage stability, which are caused by the intermittent nature of renewable power generation and the large changes in load demand. To deal with these issues, a distribution system has been designed using both short- and long-term energy storage systems such as superconducting magnetic energy storage (SMES) and pumped-hydro energy storage (PHES). The aim of this paper is to propose a metaheuristic-based optimization method to find the optimal size of a hybrid solar PV-biogas generator with SMES-PHES in the distribution system and conduct a financial analysis. This method is based on an efficient algorithm called the "enhanced whale optimization" algorithm (EWOA), along with the proposed objective functions and constraints of the system. The EWOA is employed to reduce the hybrid system's life cycle cost (LCC) and improve its reliability, both of which serve as performance indicators for the distribution system. The proposed method for sizing a grid-connected hybrid solar PV-biogas generator with SMES-PHES is compared with other metaheuristic optimization techniques, including the African vulture optimization algorithm (AVOA), grey wolf optimization algorithm (GWO), and water cycle algorithm (WCA). The numerical results of the EWOA show that the combination of a hybrid solar PV-biogas generator with SMES-PHES can successfully reduce the LCC and increase reliability, making the distribution system work better.

Keywords: distribution system; biogas generator; EWOA; solar PV; SMES; PHES; hybrid system

1. Introduction

1.1. Motivation and Incitement

Renewable energy sources (RES), such as photovoltaic (PV), wind, and hydropower systems, have started to replace traditional synchronous power generators as they are more efficient [1–4]. Traditional generators use fossil fuels and produce more greenhouse gas emissions, which have caused global warming and other problems [5]. On the one hand, RES do not use fossil fuels so they can provide clean energy without releasing greenhouse gases [6–8]. For this reason, most countries in the world are now trying to meet their growing electricity needs with renewable energy sources (RES) such as solar, wind, hydro, and biogas while making the switch to a power sector with lower carbon emissions. On the other hand, as renewable energy sources (RES) such as solar panels and wind turbines become a part of the national power grid, the way it operates has undergone significant changes [9–11]. Moreover, the outputs of renewable energy sources vary, making it difficult to rely on the entire system [12]. The intermittent nature of clean energy sources makes it difficult to provide consumers with a consistent and uninterrupted supply of electricity and puts grid operations at risk from a variety of operational and technical challenges [13].

1.2. Literature Review

An energy storage system (ESS) with RES integration can reduce RES fluctuations by improving power quality and frequency and providing other ancillary services [14,15]. In ESS structures, electrical energy is stored in a number of different ways [16–18]. Numerous electrical energy storage systems have been categorized, along with their energy conversion methodologies and efficiencies [19]. For hybrid renewable energy system (HRES) applications, a variety of energy storage technologies can be used. Among them, flywheel energy storage (FWES), supercapacitor energy storage (SCES), superconducting magnetic energy storage (SMES), and pumped-hydro energy storage (PHES) have been proven to support large-scale ESS functions with the integration of HRES [20]. The deployment of hydro energy systems (HES) is one of the most significant and successful approaches for guaranteeing stable power networks [21]. This energy storage method is desirable as it is less expensive, easier to use and deploy, and has the lowest installation cost. Besides this, due to its reliance on precise heat transfer and ambient conditions, the development of compressed-air energy storage (CAES) is extremely challenging [22]. Electromechanical energy storage such as FWES consists of a back-to-back converter, an electrical machine, a large disc, and a DC-bus capacitor [23]. The mechanical components of this type of storage system can limit its effectiveness and stability. In [24], the authors proposed a superconducting thrust-bearing system for FWES with limited loss and maintenance costs to solve a number of problems with flywheels.

Supercapacitors (SCs) are electrostatic storage devices with a high degree of recyclability and a high power density [25]. One of the few systems capable of storing direct electric energy is SMES. An SMES system consists of a cooling system, superconducting coil, electrical system, and control system for process optimization and current adaptation [26]. Two key attributes of energy storage devices are power density and energy density.

Many studies present and compare the power and energy densities of storage systems. Because of their slow dynamic response, battery energy storage (BES) and fuel cells (FCs), both ESS technologies with high energy densities, cause power control issues. In contrast, large power demands can be met by SCs and FWES, but this can reduce the storage system's lifespan [27]. None of the current storage technologies can simultaneously meet the power and energy density requirements. As a result of the limited storage technology, it is often necessary to improve the performance of hybrid energy storage system (HESS) in both "transient and steady-state" operations [28,29]. For the safest and most effective performance of a hybrid system, the appropriate technologies should be integrated with the necessary control mechanisms. In a grid-connected or standalone hybrid system, the entire design of a HESS is affected by factors such as the choice of storage technology and rated capacity, power converter topology, energy management, and control approach. Careful consideration must be given to these factors. Numerous review articles have been published on HESSs. Most recent review studies have focused on HESSs in electric cars [30–32], whereas others have concentrated on HESSs in renewable energy [33,34]. The majority of research publications investigate converter topologies, control techniques, and applications.

Depending on the purpose of hybridization, a HESS can consist of more than one energy storage system. A HESS comprises two main parts: high-power and high-energy storage systems. The high-power storage system handles or provides transient and peak power, whereas the high-energy storage system meets long-term energy needs [28,35,36]. A HESS offers several advantages when integrated into HRES, including an increase in overall system efficiency, a reduction in system expenses, and an extension of the ESS's service life [37]. For this reason, there are different types of energy storage technologies with different features. This makes it possible to combine different types of energy storage technologies in various ways. The combination of several storage systems can be employed for diverse purposes. RES applications frequently utilize HESS combinations such as BES/SC [38], BES/SMES [39,40], BES/FC [41], FC/SC [41,42], and FWES/FC [28,43]. The best HESS combinations depend on a number of factors such as the available storage space, storage costs, storage location, and specific hybridization goals.

Based on various researchers' findings in the aforementioned reviews, possible hybrid energy storage arrangements combining high-energy (long-lasting) and high-power storage (fast-response) devices have been considered [44,45]. Storage devices that provide high energy (long-lasting) include BES, CAES, FC, and PHES, and storage devices that provide high power (fast-response) include BES, SC, FES, and SMES [46]. There have been problems integrating single energy storage systems with hybrid renewable energy sources. For example, voltage and frequency fluctuations have been hard to stabilize. As technology changes, HESSs have also changed to include technologies, such as energy arbitrage, peak shaving, time shifting, and voltage support, to help them run more efficiently [42]. Adopting a comprehensive energy storage policy to balance the grid, reduce costs, and improve reliability would be significant for both renewable and traditional network systems. Other factors to consider in HESSs include how they charge and discharge (reaction time), as well as their capacity, efficiency, energy and power density, life span, and level of corrosiveness [47–49].

A review of the related literature on the application and selection of HESSs revealed a number of intriguing HESS applications, including a supercapacitor/battery HESS [50–53] and an SMES/battery HESS [54–56] in a hybrid solar PV–wind power plant system. HESSs have been used in most studies to reduce the fluctuation of wind speed and solar radiation output power [57,58]. An ESS can be incorporated to mitigate some of the issues caused by fluctuating power generation sources such as solar and wind energy. Since a HESS combines both low- and high-speed responses, it can achieve greater smoothing than a single ESS, given that wind power is comprised of several frequency components with varying amplitudes. In the reviewed literature, a similar HESS (including BES and an SC) was recommended for managing wind-energy variations in power supplies in remote regions [59]. The output regimes of solar PV and wind farms can be stabilized more effectively and efficiently by integrating sufficient sizes of hybrid fast-response and long-lasting energy storage devices. To reduce wind power variations and meet grid demands, a genetically adjusted fuzzy logic controller has been used [60]. SMES and an electrolyzer have been used to properly correct output changes in a solar and wind power plant [61].

There are two types of HESSs: standalone and grid-connected. Both grid-connected BES/SMES HESSs at the municipal, district, or regional level [62] and standalone energy supply systems based on BES/SMES for renewable energy [63] are examples of HESS applications. Many HESS applications depend heavily on batteries, especially lithium-ion batteries, which can be utilized as either "high-energy" or "high-power" storage system. SCES and FWES have even greater power densities, efficiencies, and cycle lifetimes than batteries. Redox-flow batteries are a promising technology due to their inherent decoupling of power and stored energy, extended cycle lifespan, and recycling potential. Methane (CH4) and renewable hydrogen (H2) are both excellent candidates for long-lasting energy storage. The short lifespan of electrochemical energy storage such as batteries and FC is one of its drawbacks. Battery longevity is increased and deterioration is prevented by avoiding frequent cyclic charging and draining [64,65].

By lowering the number of battery-related charge and discharge operations, smoothing the battery power profile, and eliminating supply fluctuations, it is possible to extend the battery lifespan in HESS structures [66,67]. A power management system that utilizes both lithium batteries and an SC can extend the life of a BES, with the SC fulfilling the high-frequency requirement [68]. A control mechanism was presented in [69] that can contribute to the instantaneous power between the BES and SMES. Instead of directly supplying the power fluctuations, the battery discharges and charges in accordance with the SMES current in the system. Future HESS applications will place more emphasis on heat storage and power-to-heat concepts. Through power-to-gas conversion and the storage of excess heat from renewable energy sources, the overall utilization rate of renewable energy will increase. Additionally, renewable energy systems can be cheaper, more efficient, and last longer if the design, control, and energy management techniques for HESSs at the intersection of the electricity, heat, and gas sectors are improved. Furthermore, ESS hybridization can lessen the possibility of environmental problems while enhancing operation and maintenance [70–72].

The HESS performance indicators listed above have been used to compare the technologies of energy and power storage devices for pulse applications.

Globally, energy storage devices are employed extensively. Among the most popular systems on the market are battery energy storage systems(BESSs), which utilize electrochemical processes to provide a steady electron flow in parallel or series-connected cells and store electrical energy in chemical form [73,74]. Due to their high energy density storage, convenient voltage characteristics, and small size, this technology is ideal for micro-renewable energy systems. However, BESSs are limited in terms of voltage and current, can harm the environment when chemicals are discarded after use, and have short life cycles.

Another popular technique is compressed-air energy storage (CAES), which uses compressed air to power gas turbines while storing energy as potential energy [75]. Even though this technology can produce a lot of power, it has to be installed in a particular way, has heavy start-up costs, and is expensive to run and maintain [76,77]. The third technique is FWES, which stores energy in the momentum of a rotating wheel. FWES features a very high-output power density and an extended life cycle. However, its energy density is poor, and its standby losses are considerable [44]. Previous research has shown that the above energy storage devices have a number of problems, such as a short life cycle, limited voltage and current, low energy, and poor conversion of electric energy, which can slow them down. On the other hand, SMES is mostly considered as a replacement for electricity storage and to improve the power system's transient stability, dynamic stability, and frequency management [78]. SMES uses a magnetic field that is created by a current flowing through a superconducting coil or inductor to store energy [79–81]. Other energy storage systems convert electrical energy into either chemical or mechanical energy, which is much slower than the pure electrical energy conversion of SMES. Additionally, the coil can be charged and discharged an infinite number of times [82].

A general assessment of the research indicates that SMES is anticipated to gain popularity and be used in a wide range of power applications for a speedy response [83]. When selecting one of the ESSs, it is crucial to keep in mind the service life, efficiency, and timely response in order to meet the primary goal of the SMES unit. SMES and SCES have the longest service life (around 30 years), followed by lithium-ion and sodium-sulfur batteries (around 16 years), lead-acid batteries (around 10 years), and vanadium redox batteries (around 10 years). The SMES unit is the most efficient (about 98%), followed by lithium-ion batteries (about 90%), lead-acid batteries (about 85%), supercapacitors (about 84%), and sodium-sulfur and vanadium redox batteries (about 80%). Typically, these ESSs respond within a few milliseconds [84–87]. Based on these advantages, the SMES is selected as a fast-response ESS. In addition, PHES is currently the most popular type of long-term ES technology. This type of energy storage works 70–80% of the time, and the system's capacity is not affected by changes in water flow during the different seasons [88–92]. PHES offers low installation costs, long lifespans, and low self-discharging rates [46]. When the amount of energy generated exceeds the load requirement, PHES power plants work differently than conventional hydropower plants by pushing water from the lower reservoir to the higher tank. During peak demand periods when the cost of energy is highest, the stored water is released back into the lower reservoir to power the hydraulic turbine and generator set.

1.3. Contribution and Organization of this Paper

Based on the rapid response of SMES and the long-lasting energy of PHES, these energy storage systems have been selected. Thus, implementing the cost-effective, long-term advanced technology of ESSs in grid-connected HRES applications can improve energy efficiency and stability. Selecting a suitable type and size of storage is the most crucial concern in HESS applications. Different approaches have been proposed for sizing the storage capacity. Although some methods are designed to size all types of storage regardless of technology, others can be used to estimate the HESS's capacity of a specific technology. The total cost and system reliability should be taken into account when sizing HESSs [93]. Depending on the HESS application's goal, several HESS sizing techniques can be used. Recently, researchers have used heuristic and metaheuristic optimization techniques because of the sizing problem's nonlinear objective function. It has been suggested that a modified version of the simulated annealing particle swarm optimization method can be used to solve the HESS optimization problem and determine the lowest price [94]. According to the findings, adding a HESS to a hybrid renewable power generation system can lower the overall system cost and significantly extend battery life. In this study, hybrid solar PV–biogas systems with SMES-PHES have been taken into consideration. To determine the optimal system size, the enhanced whale optimization algorithm (EWOA) and other metaheuristic optimization methods have been employed for comparisons. This paper's major contributions are as follows:

- ✓ For grid-connected hybrid solar PV–biogas systems, the optimal size is determined by considerating economic and reliability parameters.
- ✓ A customized EWOA is introduced for determining the optimal sizing of grid-connected hybrid solar PV–biogas power plants.
- ✓ A comprehensive examination is conducted of grid-connected hybrid solar PV–biogas applications, investigating the issue from a variety of perspectives, including the HESS's size, rapid responses (i.e., SMES), and long-lasting (i.e., PHES) energy characteristics.
- ✓ Comparisons between the EWOA and other metaheuristic optimization techniques for sizing energy sources and storage capacities, which consider the cost as well as reliability parameters, are carried out.
- ✓ The hybrid system's distinct instabilities can be reduced, and the load power demand can be leveled with the integration of PHES and SMES, both of which provide straightforward deployment and high effectiveness against weather variations and the inclusion or outage of RES.
- ✓ The potential and requirements for implementing grid-connected hybrid solar PV/biogas with SMES-PHES, which are also interconnected hybrid renewable energy with hybrid energy storage, are highlighted in the Debre Markos distribution network.

The present work is structured as follows. Section 2 describes the methodology, whereas Section 3 provides a description of the proposed system layout, mathematical modeling of the HRES system components, and proposed operational strategies of HRES. Furthermore, Sections 4 and 5 describe the different types of evaluation parameters and optimization techniques, respectively. Finally, Section 6 presents the results and discussion, and Section 7 presents the conclusions.

2. Methodology

The proposed system integrates a fast-response SMES system into a grid-connected hybrid solar and biogas power system, combined with a PHES system. It is used to conduct a preliminary analysis of a village's energy needs, the area's current and future renewable energy efforts, and an energy infrastructure that is easily accessible. The optimal size for each power generation method is established, considering the local economic and energy requirements.

The methods used in this study include metaheuristic optimization algorithms: the EWOA, WOA, WCA, AVOA, and GWOA. The results of these techniques are then compared.

2.1. Load Assessment

The majority of urban and suburban regions in Ethiopia receive their electricity from the national grid and struggle with poor power quality, making dependable and clean electrification a top priority. Some urban areas now have access to electricity with good power quality, while electrification projects are still in progress in other areas. The northern Ethiopian town of Debre Markos is fully electrified but has poor power quality. Figure 1 shows the hourly load profile of Debre Markos University's power distribution system. The load profile for the community on a typical day under the most severe case scenario is shown.

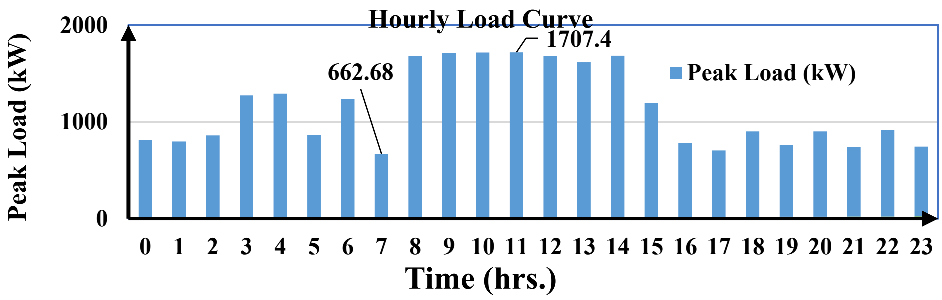

Figure 1. The community's hourly load profile on a typical day.

2.2. Renewable Energy Resource Assessment

The renewable energy sources (RESs) used in this study were solar and biogas power [95]. The examined community has nearly year-round access to solar radiation, with bright days being slightly longer in the summer and slightly shorter in the winter. In March, the surrounding temperature at the given site climbed to 25 °C. In July and August, the lowest temperatures were 16.24 °C and 16.36 °C. The chosen location's solar radiation information was retrieved from NASA's ground meteorology and solar energy database. The average yearly solar radiation in the area of study was 6.67 kWh/m^2/day. The daily solar radiation fluctuated between 5.60 kWh/m^2 and 7.80 kWh/m^2/month. The community's clearance index and changes in daily solar radiation are shown in Figure 2, indicating that the site for the chosen PV system has sufficient solar capacity.

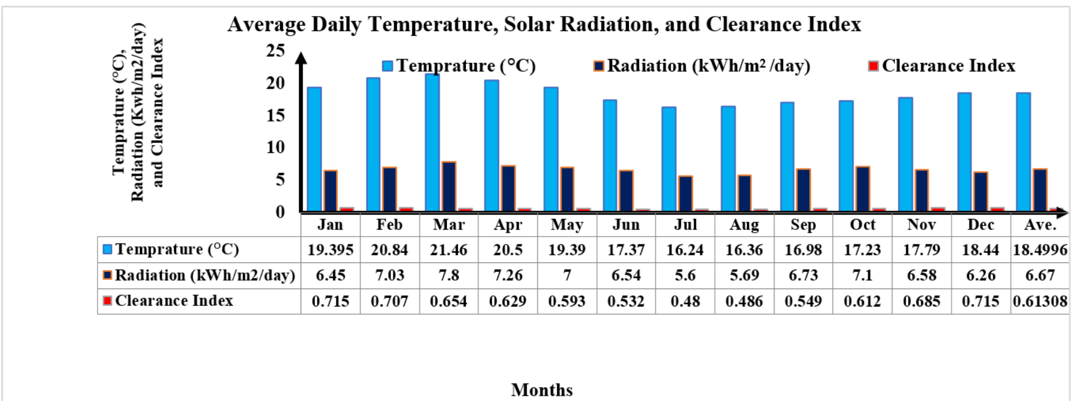

Figure 2. Average daily temperature, solar radiation, and clearance index in the study area.

The purpose of the biogas generator in this study is to prevent environmental problems that could result from the improper disposal of food waste, animal manures (including human manures), and effluent (paunch manure) from the abattoir [96,97]. This is accomplished by employing a biodigester to turn the waste materials and manures into biogas. Based on the collected data, the biogas potential for the abattoir, food, and animal waste is estimated to be 2,872,984.91 m^3/year, 2,550,105.67 m^3/year, and 2,505,634.78 m^3/year, respectively.

3. Proposed System Layout and Description

The grid-connected solar PV–biogas hybrid system, in conjunction with the SMES-PHES hybrid storage system, is considered for both short- and long-term load responses. Figure 3 depicts the proposed hybrid system, which consists of solar PV and biogas generators, a HESS with SMES and PHES, a national grid connection, and AC loads linked to the system via their respective controlled-power electronic converters. MPPT systems are used in solar PV systems to harvest the maximum amount of electricity. The PHES system, as the primary storage system, provides energy to the system when HRES production is insufficient to meet demand and consumes energy when HRES production exceeds demand. On the one hand, PHES has a high degree of dependability, but its reaction time during transient situations is poor.

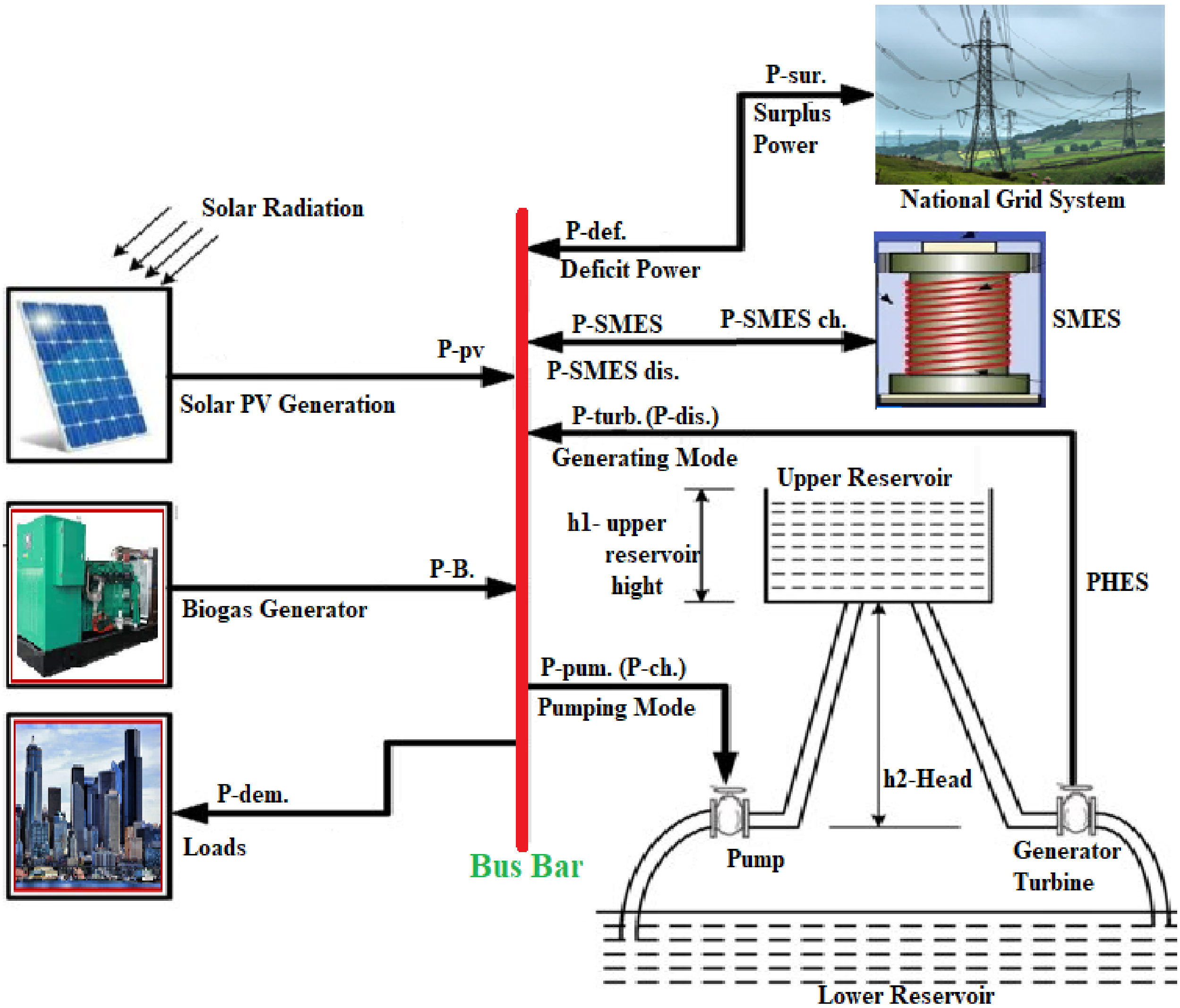

Figure 3. Schematic diagram of the proposed grid-connected solar PV–biogas hybrid system with SMES-PHES.

Therefore, SMES is used to compensate for the slow dynamics of PHES. Small- and medium-sized enterprises have been using energy from the system and supplying energy to the system. The output of a hybrid system is primarily a source of power. Assuming that converters are integrated into the system model, both the PCS and DC supply will switch to AC power. The converter transforms the SMES's direct current output into the system's alternating current. The duty cycle and the inductance current of the chopper have been set. This plant concept can be used for both distributed and grid-connected power-producing systems. If customers have a connection to the utility point, the hybrid system can then be used for both importing and exporting power. The grid then obtains power from the hybrid system when the HRESS has more power than it needs and the HESS is fully charged. However, many technical details about the HRES component pieces have not been provided.

3.1. Mathematical Modeling of Hybrid Energy Sources

A grid-connected hybrid power system composed of solar PV, biogas, and hybrid SMES-PHES could be an affordable way to generate sustainable energy that matches realistic load demands that vary over time. As a result, the unmet energy demand must be minimized at all times. This section provides an explanation of each component's modeling. Building and constructing an appropriate model, as well as scaling a hybrid system, require mathematical modeling. The following paragraph provides a detailed explanation of the mathematical modeling of each component in the hybrid system.

3.1.1. Solar PV Array Unit Modeling

The basic component of a photovoltaic array is the solar cell, which is connected in series and/or in parallel to form solar PV modules. A typical module consists of 24/72 cells connected in series. The amount of radiation, operating temperature, and level of panel cleanliness all have an impact on the photovoltaic system's output power [98]. Based on the solar radiation and surrounding temperature, a PV module's output power can be stated as [99]:

$$P_{PV}(t) = N_{PV} \times V_{OC}(t) \times I_{SC}(t) \times FF \tag{1}$$

where N_{PV} is the number of PV panels, V_{OC} and I_{SC} are the open-circuit voltage (V) and short-circuit current (A) of the solar PV panels, and FF is the fill factor. A solar PV panel's V_{OC} and I_{SC} can be computed using the following formula [99]:

$$V_{OC}(t) = V_{OCS} - \tau \times \left(T_{PV}(t) - 25^{0}\right) \tag{2}$$

$$I_{SC}(t) = \left[I_{SCS} + \varsigma\left(T_{PV}(t) - 25^{0}\right)\right] \frac{Q_{PV}(t)}{1000} \tag{3}$$

$$T_{PV}(t) = T_{amb}(t) + \frac{\left(T_{PVnm}(t) - 20^{0}\right)}{800} \times Q_{PV}(t) \tag{4}$$

where V_{OC} and I_{SC} are, under standard test conditions (STC), the open-circuit voltage (V) and short-circuit current (A), respectively. Q_{PV} denotes the global solar irradiance $\left(W/m^2\right)$ incident on the solar panels, τ is the open-circuit voltage temperature coefficient $(V/°C)$, ς is the short-circuit current temperature coefficient $(A/°C)$, T_{amb} is the operating temperature of the solar cell, and T_{PV} is the nominal temperature of the solar cell in $°C$. Additionally, the solar PV panel's FF is calculated as follows:

$$Fill factor(FF) = \frac{V_{mpp} \times I_{mpp}}{V_{OC} \times I_{SC}} \tag{5}$$

where V_{mpp} and I_{mpp} represent, respectively, the voltage and current at the maximum power point.

The energy produced by the PV system ($E_{PV}(t)$) at hour "t" is calculated as:

$$E_{PV}(t) = P_{PV}(t) \times \Delta t \tag{6}$$

The maximum power point tracking (MPPT) system's efficiency is closely linked to the PV modules' efficiency. According to [100], including an MPPT system in hybrid systems is economically possible because it will boost the energy produced by the photovoltaic modules by roughly 30%. As a result, it is assumed that the PV modules in the system under investigation are fixed on a tracking system with an efficiency of 95%.

3.1.2. Biogas Generator (BG) Unit Modeling

The biogas generating system's output power (PB(t)) is calculated using the following equation [99,101]:

$$P_B(t) = \frac{Q_G \times F_G \times \eta_G}{860 \times H_G} \tag{7}$$

where Q_G is the daily biogas availability (m^3/day), F_G is the calorific value of biogas (4700 kcal/m^3), and η_G is the total efficiency of converting biogas into power (35%). H_G is the number of hours that the biogas generator is open each day. The energy $(E_B(t))$ produced by the biogas generator system at hour 't' is calculated as:

$$E_B(t) = P_B(t) \times \Delta t \tag{8}$$

3.1.3. Hydraulic Pumped-Storage System Modeling

The amount of water flowing through a turbine is measured in m^3/s. Generally, the formula below is used to determine how much energy is produced at a hydroelectric power station [102]:

$$E_H = \eta_H \times \rho \times g \times Q \times h \times \Delta t \tag{9}$$

where E_H is the amount of energy that a water turbine produces (kWh), η_H is the efficiency of the water turbine and generator (%), ρ is the density of the seawater (kg/m^3), g is the acceleration of gravity (m/s^2), Q is the quantity of water flowing through the turbines (m^3/s), and h is the effective head (m).

The volume of stored energy is considered the reservoir's maximal capacity. It is expected that the amount of water that is stored during the simulation period must not be less than the minimum permissible value $V_{\min}$. The amount of energy set aside is calculated as a share of the higher reservoir's maximum capacity. The following formulae can be used to compute the volume of water that is kept in the tank at any given time of the year:

$$\begin{array}{l} if \begin{cases} V_{\max} - V_{(t-1)} < V_{\min} \\ V(t) = V_{(t-1)} - Q^{dis}_{(t)} + Q^{pump}_{(t)} \end{cases} \\ else \Big\{ V(t) = \min\Big(V_{(t-1)}; V_{\max}\Big) - Q^{dis}_{(t)} + Q^{pump}_{(t)} \end{array} \tag{10}$$

where $V_{\max}$ and Q^{dis} are the upper reservoir's maximum capacity (m^3) and the amount of water that comes out of the tank per second (m^3/s). Both are used to meet the load demand when solar and biogas power are low. Q^{pump} is the amount of water pumped from the sea into the upper reservoir (m^3/s) by solar and biogas power plants when the system has excess energy.

In generating mode, the system calculates how much electricity the generator and turbine set produce. When the energy balance value is less than zero, the system can be in generating mode, according to Equation (11).

$$E^H_{(t)} = \min\left[\min\left(\frac{V_{(t-1)}}{3600}; Q_T\right)\eta_T \eta_{WP} \rho g (h_{add} + h_3); |E_B|\right] \tag{11}$$

where η_{WP} and η_T are the efficiencies of the pipeline and the generator, h_3 is the average head of the PHES system, and Q_T is the discharge water from the upper reservoir that exits the turbine (m^3/s). The volume of water expelled at that time is given in the following equation, which is derived from the previous equation:

$$Q^{dis}_{(t)} = \frac{E^{H}_{(t)}}{\eta_T \eta_{WP} \rho g (h_{add} + h_3)} \tag{12}$$

The hybrid system may or may not be able to meet all the energy needs. The system may need help from the grid to meet the energy needs. Equation (13) can be used to estimate the energy deficit in this case:

$$E^{def}_{(t)} = \left| E^{B}_{(t)} + E^{H}_{(t)} \right| \tag{13}$$

When the value of the energy balance is $E_B > 0$, the excess energy is used to move water from the sea to the upper water reservoir. In this case, the electric energy used by the pump system at any given time is computed using the formula:

$$E^{pump}_{(t)} = \min\left[\min\left(\frac{V_{\max} - V_{(t-1)}}{3600}; Q_P \right) \eta_P \eta_{WP} \rho g (h_{add} + h_3); |E_B| \right] \tag{14}$$

where η_P denotes the pumping unit's efficiency and Q_P denotes the pumping speed (m^3/s). The following formula computes the charging water from the lower reservoir to the upper reservoir at a specific time, and is based on the previous equation:

$$Q^{pump}_{(t)} = \frac{E^{pump}_{(t)}}{\eta_P \eta_{WP} \rho g (h_{add} + h_3)} \tag{15}$$

3.1.4. Superconducting Magnetic Energy Storage (SMES) System Modeling

SMES was used as the energy storage solution because of its rapid responsiveness and extremely high efficiency (charge-discharge efficiency exceeding 95%) [103–105]. Depending on the demand requirements, the power stored in the coil can be charged or discharged. Load leveling, damping control, and load frequency control are all ways that SMES can be used in power systems [106–108]. SMES systems are usually used to store energy for short periods in data centers, hospitals, military bases, and industries [109]. In short, SMES systems can store the surplus or excess energy generated by HRES, rather than wasting it when the load demand is low, and release energy to supply peak load demands throughout the day. In other words, SMES system can function as loads during charging mode to store energy and as generators during discharging mode to release or deliver energy. The three operational states are charging mode, discharging mode, and standby mode, which are expressed as follows:

1. **Charging Mode of Operation:** This mode occurs when HRES power generation is higher than the load demand PL (i.e., PL − P_{HRES} < 0 or $P_{\text{SMES Ex.}}$(t) < 0).

$$P_{\text{SMES Ex.}}(t) = \max\left\{ -|\Delta P(t)|, \frac{(E_{\text{SMES St.}}(t-1) - E_{\text{SMES, max.}})}{\Delta t \times \eta_{Cha.}}, -P_{\text{SMES, rated}} \right\} \tag{16}$$

$$E_{\text{SMES St.}}(t) = \min\{ (E_{\text{SMES St.}}(t-1) - P_{\text{SMES, Cha.}}(t) \times \Delta t \times \eta_{Cha.}), E_{\text{SMES, max.}} \} \tag{17}$$

2. **Discharging Mode of Operation:** This mode occurs when the load demand PL is higher than the HRES power generation (i.e., PL − P_{HRES} > 0 or $P_{\text{SMES Ex.}}$(t) > 0).

$$P_{\text{SMES Ex.}}(t) = \max\left\{ |\Delta P(t)|, \frac{(E_{\text{SMES St.}}(t-1) - E_{\text{SMES, min.}}) \times \eta_{Cha.}}{\Delta t}, -P_{\text{SMES, rated}} \right\} \quad (18)$$

$$E_{\text{SMES St.}}(t) = \max\left\{ E_{\text{SMES St.}}(t-1) - \left(\frac{P_{\text{SMES, Dis.}}(t) \times \Delta t}{\eta_{Dis.}} \right), E_{\text{SMES, min.}} \right\} \quad (19)$$

3. **Standby Mode of Operation:** This mode occurs when the load demand PL is equal to the HRES power generation (i.e., PL $-P_{HRES}$ = 0 or $P_{SMES\ Ex.}$(t) = 0). The SMES system must run in standby mode to maintain the stored energy in the system when it is not necessary for it to exchange power with the primary DC-bus bar.

where $P_{SMES\ Ex.(t)}$ is the exchanged power of SMES at period t, which is negative, positive, and equal to zero during charging mode, discharging mode, and standby (idle) mode, respectively; $\eta_C$ha. and $\eta_D$is. are the efficiencies of charging and discharging modes, respectively; ΔP(t) is the difference between the output and load demand of HRES; $P_{SMES,rated}$ is the power rating of SMES; $E_{SMES\ St.}$(t) is the energy storage capacity of SMES at period t; $E_{SMES,min.}$ and $E_{SMES,max.}$ are the minimum and maximum energy storage capacity limits of the SMES system, respectively; and Δt represents the time interval.

3.1.5. Modeling of Converter

The main function of the inverter is to transform the DC power from solar PV and battery power into AC power and to send more power to the grid than is allowed. According to [110], it is assumed in this analysis that the inverter efficiency (η_{inv}) is 90% as a fixed value. As a result, the equation below can be employed to estimate the inverter's output power:

$$P_{inv-AC} = (P_{SMES-inv} + P_{PV-inc}) \times \eta_{inv} \quad (20)$$

where $P_{SMES-inv}$ is the output power from the SMES system, and P_{PV-inv} is the power generated from the solar PV sources.

3.2. Operation and Energy Management Strategy

The operation of the proposed hybrid renewable system is summarized in the following operational scenarios. A flowchart outlining the hybrid system's operational philosophy is shown in Figure 4. The power supply system can be seen to vary as the load demand changes. In addition, the supply changes based on the load demand. When the load demand increases, the system's power supply (production) also increases by the same amount. In light of this, the distribution system's power stability problem can be managed. Consequently, the power supply must be capable of keeping up with sudden, rapid load variations. Thus, when the load demand increases, the power supplied by the hybrid system also increases, whereas when the load demand decreases, the power supply also decreases or is disconnected from the grid-connected hybrid power system. A hybrid system works best when it can respond in milliseconds to variations in the power production minus the load demand. It supplies electricity to the system until long-term energy storage, such as PHES, or a biogas generator begins to cater to the connected load. However, before SMES can function, a comparison between the superconducting coil's inductor current (I_{SMES}) and its lower limit of the inductor current ($I_{SMES}dL$) must be made.

If the coil current surpasses $I_{SMES}dL$, the SMES system discharges and delivers power to the grid-connected hybrid system. In another scenario, when the gap between the amount of power produced and the amount needed is greater than zero, the SMES system keeps running until a long-term energy storage system or other energy sources can meet the connected demand. The SMES system's inductor coil current reaches its limit for part of the extra power that was sent to the SMES system before it was charged. Therefore, the SMES system operates in charging mode and uses energy from the grid-connected HRES if the inductor current is less than the upper limit; otherwise, the SMES system cannot charge. The SMES system stays in standby mode, meaning it is neither charging nor discharging when there is no difference between the change in power production and the load demand. However, long-lasting energy storage systems such as PHES and SMES both have the same commands.

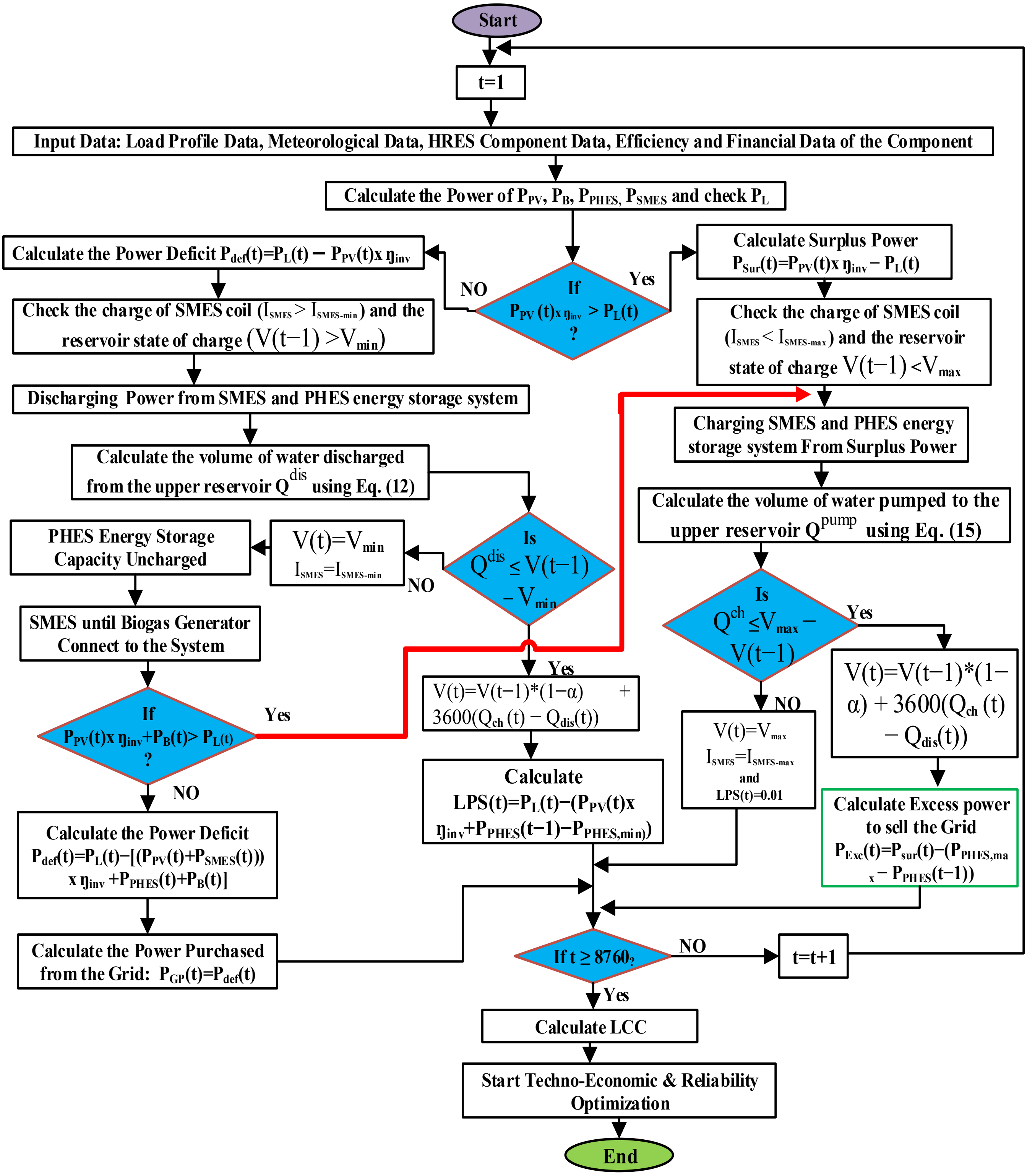

Figure 4. Flowchart showing the operation of the proposed grid-connected hybrid solar PV–biogas system with a battery.

The proposed hybrid system functions to meet load demand because the primary energy sources are the PV panels and the biogas generator, whereas the fast-response storage system (SMES) and long-lasting energy storage system (PHES) both function to maintain the reliability and continuity of the power supply to the loads. Renewable energy sources have intrinsic limitations; therefore, the system's power generation capacity cannot be increased to meet demand on a moment-by-moment basis. As a result of the changing nature of solar radiation, managing the power in a hybrid system can be difficult. Coordinating the flow of power across all units with regard to timing and demand is important for grid-connected hybrid power generation systems. According to Salman et al. [111], there are circumstances where the amount of energy generated exceeds the amount of energy needed and the storage units are charged to capacity. In this situation, the national grid receives all the excess energy, protecting the storage systems from being overcharged [112]. Based on the aforementioned circumstances and the flowchart in Figure 4, the proposed power management strategy takes into account the following modes of operation [113,114]:

Mode I: The solar PV and biogas generator provides a considerable amount of energy, and any excess energy is used to charge the storage units if the charge level is below nominal.

Mode II: When the charge level is equal to nominal, energy is generated in excess of what is needed for the load and storage unit. All excess energy is transferred via the national grid, which is interconnected.

Mode III: The amount of energy generated by the hybrid solar PV–biogas generator is insufficient to meet demand. In terms of the importance of the operation, the following two sub-scenarios can be considered:

a. The connected electric load requirement can be met by stored energy from the hybrid SMES-PHES system.
b. If the energy in the storage units runs out, the connected national grid provides the required electric load demand.

4. Parameter Evaluation of the Optimization

4.1. Economic Evaluation

"Cost of electricity" (COE) is a widely used method for calculating the economic benefit of a hybrid renewable energy system [113]. It is written in Equation (32) as the "net cost per unit of electrical energy" [115]. In this study, the COE produced by the suggested hybrid renewable power system is reduced while providing a consistent supply of electricity to the consumer. The system's total annual cost (TAC) is considered in the economic analysis.

$$TAC = C_{ann,cap} + \sum_{i=1}^{T=8760} C_{O\&M} + \sum_{i=1}^{T=8760} C_R \tag{21}$$

where C_R is the replacement cost of each subsystem, $C_{O\&M}$ is the cost of operation and maintenance of each subsystem, and $C_{ann,cap}$ is the annual interest of the capital cost.

The net present cost (NPC) describes the present value of the capital investment and the operating costs over the lifetime of the project and can be expressed as follows [116]:

$$NPC = \frac{TAC}{CRF} \tag{22}$$

where CRF is the capital recovery factor.

The CRF is used when converting the initial investment cost to the annual capital cost. The CRF can be calculated by:

$$CRF(r, n) = \frac{r(1+r)^n}{(1+r)^n - 1} \tag{23}$$

where r is the interest rate (12%) and n is the length of time the proposed hybrid system is expected last (25 years). The COE (EUR/kWh) is how much it costs the system to produce one kWh. The COE is calculated as follows:

$$COE = \frac{NPC}{\sum_{T=1}^{T=8760} P_{load}(t)} \times CRF \tag{24}$$

The levelized cost of energy (LCOE) is a method for estimating the amount of money spent on energy per kilowatt-hour (EUR/kWh) for the duration of the project.

The cost per kWh of various power system technologies is compared using the LCOE. Estimating the LCOE involves dividing the project's lifecycle cost by its anticipated energy output from HRES [117]. The LCOE can be calculated as follows:

$$LCOE = \frac{LCC}{E_{Generation}} \tag{25}$$

where $E_{Generation}$ is the system energy generation and LCC is the lifecycle cost of the project. The cost of replacement is lower than the salvage value, which implies that the cost of the project over its lifetime is equal to the value of the project at the end of the system's life. It also includes the initial capital, operation, and maintenance costs. The LCC can be calculated using the following formula:

$$LCC = C_{cap} + \sum_{T=1}^{T=8760} C_{O\&M} + \sum_{T=1}^{T=8760} C_R - C_{Sal} \tag{26}$$

where C_{cap}, $C_{O\&M}$, C_R, and C_{Sal} represent the capital, operation and maintenance, replacement, and salvage costs for the project's end-of-life value, respectively.

The salvage cost (C_{Sal}) is the value of an integrated system's components at the project's conclusion. The salvage cost is calculated as follows [118]:

$$C_{Sal} = C_R \times \frac{R_{rem}}{R_{PL}} \tag{27}$$

where R_{rem} and R_{PL} denote the components' remaining life and project lifespan, respectively.

4.2. Reliability Evaluation

The capability of an electrical power system to deliver sufficient energy to a given load without any shortage or interruption in service is referred to as system reliability. The expected energy not supplied (EENS) index, reliability index (RI), and loss of power supply probability (LPSP) index are the three most commonly used system reliability indices [119,120]. These indices reveal how well the load is distributed. Using Equation (28), one can obtain an estimate of the EENS [121].

$$EENS = \sum_{t=1}^{8760} [P_{load}(t) - (P_{PV}(t) + P_B(t) + P_{SMES-dis}(t) + P_{PHES-dis}(t) - P_{SMES-cha}(t) - P_{PHES-cha}(t))] \tag{28}$$

In this study, the LPSP must be less than a predetermined value of 1%. The LPSP is determined according to Equation (29) [122]:

$$LPSP = \frac{\sum_{t=1}^{8760} [P_{load}(t) - (P_{PV}(t) + P_B(t) + P_{SMES-dis}(t) + P_{PHES-dis}(t) - P_{SMES-cha}(t) - P_{PHES-cha}(t))]}{\sum_{t=1}^{8760} P_{load}(t)} \tag{29}$$

As shown in Equation (30), the RI indicates the ability of HRES to meet the load demand without service interruptions [123].

$$IR = 1 - \left[\frac{\sum_{t=1}^{8760} [P_{load}(t) - (P_{PV}(t) + P_B(t) + P_{SMES-dis}(t) + P_{PHES-dis}(t) - P_{SMES-cha}(t) - P_{PHES-cha}(t))]}{\sum_{t=1}^{8760} P_{load}(t)}\right] \tag{30}$$

The loss of load probability (LOLP) can be computed by dividing the number of hours when the power of the load demand exceeds the combined power coming from renewables and grid purchases by the total time in hours, which is 8760, as shown in Equation (31) [124].

$$LOLP = \frac{\sum_{t=1}^{8760} hours\#at\left[\left(P_L(t) + P^{cha}_{PHES\&SMES}(t)\right) > \left(P_{PV}(t) + P_B(t) + P^{dis}_{PHES\&SMES}(t) + P_{GP}(t)\right)\right]}{8760} \tag{31}$$

4.3. Formulation of Objective Function to Optimize the Problem

The aim of this study is to reduce the life cycle cost (LCC) of a grid-connected solar–biogas generator hybrid system with SMES-PHES while maintaining high reliability of the power supplied to the connected loads and minimizing the LPSP and excess energy consumed in the interconnected national grid. For this optimization problem, the important variables are the reservoir capacity of the PHES system in m^3, the number of solar PV panels, the capacity of the biogas generator, and the capacity of the SMES system.

$$\min LCC = \min\left(C_{initial} + C_{replace} + C_{O\&M}\right) \tag{32}$$

4.4. Constraints

Several system constraints are described below, which are aligned with the aforementioned objective function. The proposed grid-connected hybrid power plant will be subject to the following limits on system sizing in order to ensure minimal costs and high reliability:

$$P_{inv}(t) \geq P_{PV\_peak}(t) + P_{SMES-dis}(t) \tag{33}$$

$$P^{\min}_{Bio}(t) \leq P_{Bio}(t) \leq P^{\max}_{Bio}(t) \tag{34}$$

$$N^{\min}_{PV} \leq N_{PV} \leq N^{\max}_{PV} \tag{35}$$

$$LPSP \leq \beta_L \tag{36}$$

where N^{min}_{PV} and N^{max}_{PV} represent the minimum and maximum limits of the PV panels, and $P^{\min}_{Bio}(t)$ and $P^{\max}_{Bio}(t)$ represent the minimum and maximum limits of the capacity of the biogas generator with high reliability or a minimum loss of power supply probability $\beta_L \leq 0.01$.

5. Optimization Technique

The proposed metaheuristic optimization technique is the enhanced whale optimization algorithm (EWOA) which is discussed and analyzed in this section. The outcomes of the chosen algorithm optimization were compared with those of other metaheuristic optimization algorithms. The algorithms were executed using MATLAB. This section includes a brief description of the proposed EWOA metaheuristic optimization algorithm used.

In 2016, Mirjalili and Lewis [125] proposed the whale optimization algorithm (WOA), a novel metaheuristic optimization algorithm inspired by the social behavior of humpback whales. The bubble-net hunting strategy was the algorithm's foundation. Although the WOA has a rapid convergence rate, it is inefficient in locating the global best solution for multimodal problems that have multiple local optimal solutions. The enhanced whale optimization algorithm (EWOA) was developed by Nadimi-Shahraki et al. in 2022 [126] as a means to improve the global search capability. By using a pooling mechanism and three efficient search techniques, the EWOA improves the performance of the traditional WOA. These strategies include migration, preferred selection, and enhancing the nearby prey. In order to sustain the genetic diversity of the population, the worst answers from each iteration are crossed with the best solutions from the pooling technique.

In addition, new search techniques have been found to complement the search strategies used in the classic WOA. In this section, a technique for pooling resources, as well as three productive search algorithms, is explored.

a. **Pooling mechanism:** Using Equation (37), the member pools $Pool = (P_{i,1}, P_{i,2}, \ldots . P_{i,D})$ of a size matrix $Pool = (P_1, P_2, \ldots P_k)$ are generated, where X^t_{brnd} is computed using Equation (39) to generate a random location near the best humpback whale X^t_{best}, and X^t_{worst} is the worst solution found in the current iteration. In this equation, B^t_i is a binary random vector, and $\overline{B^t_i}$ is its inverse vector. The values of non-zero elements in B^t_i are zero in $\overline{B^t_i}$, and the values of zero elements are equal to one. For variety, the pooling method uses a crossover operator to mix the worst and best solutions. When the pool is full, an existing pool member takes the place of the new member.

$$P^t_i = B^t_i \times X^t_{brnd} + \overline{B^t_i} \times X^t_{worst} \tag{37}$$

b. **Migrating search strategy:** Using Equation (38), this search method randomly partitions a portion of the humpback whale to explore uncharted territory and improve the exploration process. The partitioned whale populations are also anticipated to diversify, which may lessen the likelihood of local whale trapping. Equation (39), where rand is a random number between 0 and 1, and $\delta_{\min}$ and $\delta_{\max}$ are the lower and upper limits of the problem, determines X^t_{rnd} as a random point in the search space. Equation (40) is used to find the best humpback whale, X^t_{best}, and is a random location nearby. In this case, $\delta_{best\_\min}$ and $\delta_{best\_\max}$ are the lower and upper limits of X^t_{best}, respectively.

$$X^{t+1}_i = X^t_{rnd} - X^t_{brnd} \tag{38}$$

$$X^t_{rnd} = rand \times (\delta_{\max} - \delta_{\min}) + \delta_{\min} \tag{39}$$

$$X^t_{brndi} = rand \times (\delta_{best\_\max} - \delta_{best\_\min}) + \delta_{best\_\min} \tag{40}$$

c. **Preferential selection search strategy:** In the classical WOA, the prey search method can explore more effectively with the help of the preferred selection technique. This method is shown in Equation (42), where X^t_i is the current location of the ith whale, and P^t_{rnd1} and P^t_{rnd2} are randomly chosen from the matrix. In iteration t, C^t_i is defined using Equation (41), and A^t_i is sampled using a Cauchy distribution with parameters. By dispersing the whales across the search space, a diverse range of solutions can be found. However, a larger step size is recommended for the preferential selection search method to improve the WOA's ability to explore. In this method, the heavy-tailed Cauchy distribution is used because it has a higher chance of generating larger values.

$$C^t_i = 2 \times rand \tag{41}$$

$$X^{t+1}_i = X^t_i + A^t_i \times \left(C^t_i \times P^t_{rnd1} - P^t_{rnd2}\right) \tag{42}$$

d. **Enriched encircling prey search strategy:** The WOA's encircling prey method is enriched using Equation (42), where $D^{!t}$ is computed using Equation (43) and is chosen at random from the matrix pool.

$$X^{t+1}_i = X^t_{best} - A^t_i \times D^{!t} \tag{43}$$

$$D^{!t} = \left|C^t_i \times X^t_{best} - P^t_{rnd3}\right| \tag{44}$$

The source code of the EWOA is shown below (Algorithm 1).

Algorithm 1. The source code of the EWOA.

Input: Population size (N) and maximum iterations ($\mathrm{Itr_{Max}}$)
Output: The optimal solution
Begin
Distribute N wheels randomly in the future space using the equation:
$b^t_{i,j} = \begin{cases} 1, rand \geq 0.5 \\ 0, rand < 0.5 \end{cases}, i = 1,2,\ldots.N, and, j = 1,2,\ldots D$
Evaluate the fitness of the wheels using the equation:
$Fit^t_i = \alpha \times CE^t_i + \beta \times \left(\frac{FS^t_i}{D}\right),\ where,\ CE^t_i = \frac{1}{K}\sum_{Fold=1}^{K}\frac{1}{N_{Smp}}\sum_{S=1}^{N_{Smp}}\sqrt{\left(y_s - \dot{y}_s\right)^2}.$
Set t = 1
While $t < Itr_{Max}$
Randomly select a portion P of the population and compute $X^{t+1}_{i\in P}$ using the migrating search strategy.
If i is not in P
Compute the probability rate ρ^t_i and coefficient A^t_i using the equation:
$A^t_i = 2 \times \alpha^t_i \times rand - \alpha^t_i,\ where,\ \alpha^t_i = 2 - t \times \left(\frac{2}{Itr_{Max}}\right).$
If $\rho^t_i < 0.5$
If $A^t_i < 0.5$
Compute X^{t+1}_i using the enriched encircling prey strategy defined in the equation:
$X^{t+1}_i = X^t_{best} - A^t_i \times D'^t, where, D'^t = \left|C^t_i \times X^t_{best} - P^t_{rnd3}\right|$
Else
Compute X^{t+1}_i using the preferential selection strategy defined in the equation:
$X^{t+1}_i = X^t_i + A^t_i \times \left(C^t_i \times P^t_{rnd1} - P^t_{rnd2}\right)$
end if
Else
Compute X^{t+1}_i using the spiral bubble-net attacking strategy defined in the equation:
$X^{t+1}_i = D'^t \times e^{lb} \times \cos(2\pi l) + X^t_{best}$ where $D'^t = \left|X^t_{best} - X^t_i\right|$
end if
Apply the following equations in order to map the continuous search space to the binary one:
$U\left(X^t_{ij}\right) = \alpha \times \left|X^\beta_{ij}\right|$ and $b^t_{ij} = \begin{cases} 1, U\left(X^t_{ij}\right) \geq rand(0,1) \\ 0, U\left(X^t_{ij}\right) < rand(0,1) \end{cases}$
Update and evaluate the fitness of X^{t+1}_i using the equation:
$Fit^t_i = \alpha \times CE^t_i + \beta \times \left(\frac{FS^t_i}{D}\right), where, CE^t_i = \frac{1}{K}\sum_{Fold=1}^{K}\frac{1}{N_{Smp}}\sum_{S=1}^{N_{Smp}}\sqrt{\left(y_s - \dot{y}_s\right)^2}$
Update X^{t+1}_i using the position with a lower fitness value from $\left\{X^t_i, X^{t+1}_i\right\}$
end if
Update the global optimal solution
t = t + 1
end while

This section adopts the modified whale optimization method to address hybrid renewable energy source sizing issues. The proposed EWOA is compared with the most commonly used metaheuristic optimization techniques, including the AVOA, WCA, and GWOA.

6. Results and Discussion

The city of Debre Markos in northern Ethiopia was the subject of this research. This area was used to evaluate the size of a grid-connected hybrid solar PV and biogas system with SMES-PHES mechanisms. Based on the primary and secondary data acquired from various sources, the site's potential to produce biogas was estimated. The research area's biogas potential was determined to be 7.9287×10^6 m^3/year based on the collected data. In 2019, Suhartini S. et al. [127] examined the possibility of producing 2.14 kWh of energy from 1 m^3 of biogas using a biogas generator. With the estimated biogas potential, it was found that 1293.0080 kW of power and 11.3268×10^6 kwh of energy per annum could be produced.

Based on the available data, in our research area, the average annual horizontal solar radiation was 6.6732 kWh/m^2/day, and the average ambient temperature was 18.5001 °C. Figure 5 displays the hourly meteorological data over one year. Additionally, Table 1 presents the technical and financial details of the PV, SMES, inverter, PHES, and biogas generator employed in this study. In this study, the rate of interest was set to 12%, and the system's duration was set to 25 years.

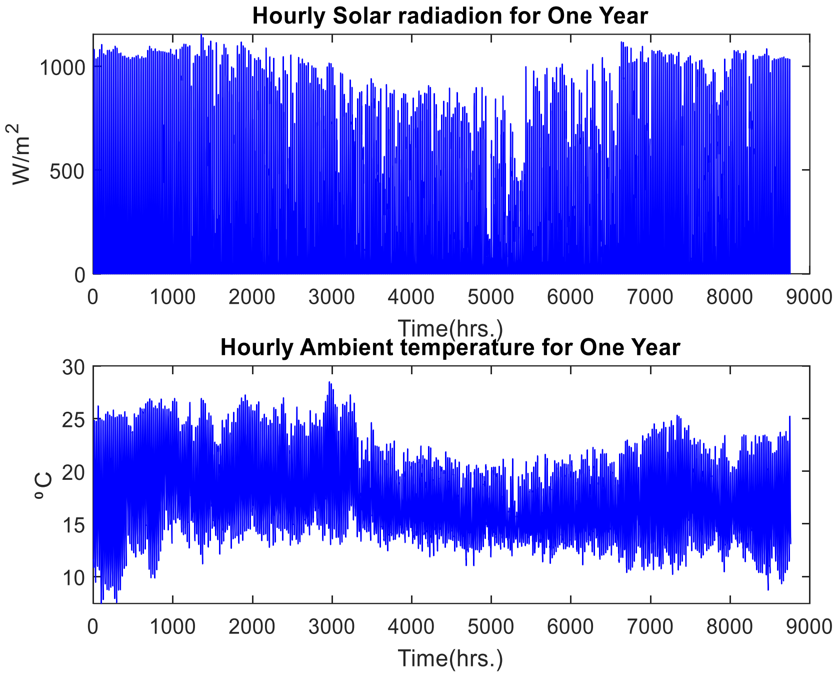

Figure 5. Data on the research area's hourly temperature and solar irradiation over one year.

Table 1. Technical and financial specifications of the HRES system's components.

Solar panel	[128]
Max power	380 Wp
Length x width	1.976 × 0.991 m
Efficiency	19.41%
Temperature coefficient	0.41%
Initial cost	145.845 EUR/kW
O and M cost	1%
Life span	25 Years
SMES	[129]
Energy, ESMES	1 MJ
Inductance, LSMES	0.5 H
Current, ISMES	1 KA
Voltage, Vdc-link	2 KV
Capacitance, Cdc-link	0.01 F
PHES	[130,131]
Overall efficiency	77%
Cost of power conversion	165–740 EUR/kW
Fixed O and M cost	8.5 EUR/kW
Variable O and M cost	0.8 EUR/MWh
Life Span	30 years

Table 1. *Cont.*

Biogas generator	[132]
Initial Cost	1342.5 EUR/kW
Fixed O and M cost	71.65 EUR/kW
Variable O and M cost	20.7 EUR/MWh
Inverter	[133,134]
Model	UnderstandSolar
Initial cost	172 EUR/kW
O and M cost	1%
Efficiency	95%
Economic parameters	
Real discount rate	12%
Lifetime of the project	25 Years

6.1. Results of Optimal Sizing of Hybrid Components

Table 2 illustrates the optimal component capacities in various hybrid system configurations using different metaheuristic techniques. The net present costs and the objective function (LCC) were both taken into account when selecting the hybrid system's appropriate size. For this hybrid system configuration, the following capacities were determined to be appropriate using the EWOA: 5496 solar PV panels, 860.29 KW for the biogas generator capacity, 400.67 KW for the PHES, 26,798.14 m^3 for the upper reservoir capacity, and 142.28 kWh for the SMES capacity. The EWOA was also found to be the most effective in determining the optimal sizes for this hybrid renewable energy system when the results from the six metaheuristic optimization methods were compared. The EWOA determined the optimal sizes for the solar PV, PHES, SMES, and biogas generators by considering the objective function (i.e., LCC) and the constraints. Additionally, the lowest values of the LCC were achieved.

Table 2. Optimized capacities of components with parameters using different metaheuristic optimization algorithms.

Technique	Type of Renewable Energy Resource				
	No. of PV Panels	**PHES Capacity (KW)**	**Reservoir Capacity (m^3)**	**Capacity of Biogas (KW)**	**SMES Capacity (KWh)**
EWOA	5495.44	400.67	26,798.14	860.29	142.28
AVOA	2928.58	346.97	25,296.88	999.94	142.28
GWOA	2964.31	349.86	24,975.71	997.63	142.28
WCA	5117.57	396.92	27,597.56	869.33	142.28

6.2. Results of Analysis of Financial and Reliability Parameters

As discussed in the previous sections, the objective function of this study was the cost (i.e., LCC) of the proposed hybrid system. Table 3 compares the results of the EWOA to those of more recent optimization methods.

As seen in Table 3, the EWOA estimated the optimal solution (minimum LCC of the project) of EUR 4.507×10^6 within the predefined operational iterations and LPSP values. In addition, the GWOA, AVOA, and WCA achieved LCC values of EUR 4.511×10^6, EUR 4.515×10^6, and EUR 4.509×10^6, respectively, within the predefined iterations and LPSP values. Moreover, the COE value was the lowest when the EWOA was applied. Chong Li et al. (2022) [135], who investigated hybrid solar–biogas energy storage systems, obtained a COE of 0.22 EUR/kWh, which was 16% higher than that of our proposed system. Furthermore, Mwakitalima et al. (2023) [136] introduced a hybrid solar–biogas energy storage system and obtained a COE of 0.082 EUR/kWh, which was higher than the 2.25% of our proposed system.

Table 3. Economical and reliability results of different metaheuristic optimization techniques.

Techniques	Financial Parameters			Reliability Parameters		
	LCC (EUR)	COE (EUR/kWh)	NPC (EUR)	LOLP (%)	EENS (KW)	IR
EWOA	4.507×10^6	0.059513	7.189×10^6	3.804	1.124×10^5	0.990066
AVOA	4.515×10^6	0.059517	7.193×10^6	4.533	1.176×10^5	0.990001
GWOA	4.511×10^6	0.059794	7.203×10^6	3.884	1.166×10^5	0.990003
WCA	4.509×10^6	0.059781	7.202×10^6	4.043	1.184×10^5	0.990066

From the results shown in Table 3, it can be seen that the EWOA predicted the lowest COE and NPC values of 0.059513 EUR/kWh and EUR 7.189 $\times$ 10^6, respectively. The COE and NPC values estimated using the GWOA were EUR 0.059794 EUR/kWh and EUR 7.203 $\times$ 10^6, and those estimated using the AVOA were 0.059517 EUR/kWh and EUR 7.193 $\times$ 10^6. The COE and NPC values estimated using the WCA were 0.059781 EUR/kWh and EUR 7.202 $\times$ 10^6, respectively. Therefore, the EWOA achieved the optimal values of the COE and NPC for the proposed grid-connected hybrid system. In addition, the EWOA achieved the lowest LOLP and EENS values, and the highest RI value, indicating a more reliable system. Fluctuations in the levels of energy injected into the grid were also minimized. The financial analysis was highly affected by the numerical values of the constraints and the participation rate of the hybrid renewable energy generation. Figure 6 illustrates the optimal results of the EWOA in terms of the NPC and COE values.

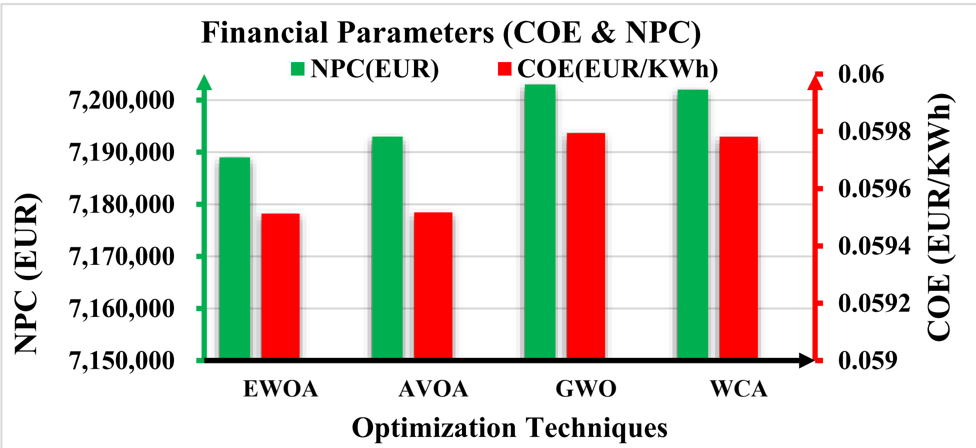

Figure 6. Graphical representation of the COE and NPC values obtained using the EWOA, AVOA, GWOA, and WCA.

Figure 7 shows that the EENS and LOLP values achieved by the EWOA were the lowest and the RI was the highest.

Overall, the outcomes of this study's objective functions indicate that EWOA outperformed the other methods in all aspects. The convergence rates of the algorithms used in optimizing the grid-connected hybrid renewable energy system under study are illustrated in Figure 8. The EWOA can be seen to have the fastest convergence rate among the considered methods, with all methods converging to the minimal COE vs. operational iterations. Moreover, the algorithms themselves rather than the decision variables determined the convergence rates.

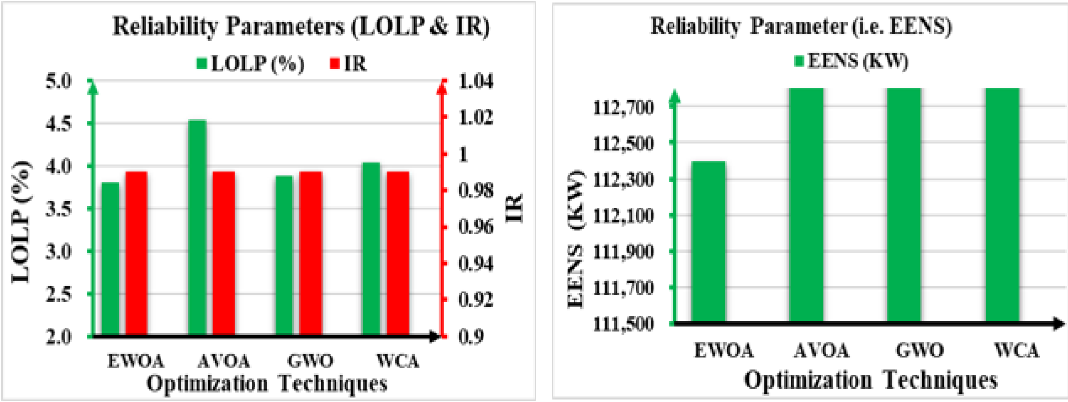

Figure 7. Graphical representation of the LPSP, RI, and EENS values obtained using the EWOA, AVOA, GWOA, and WCA.

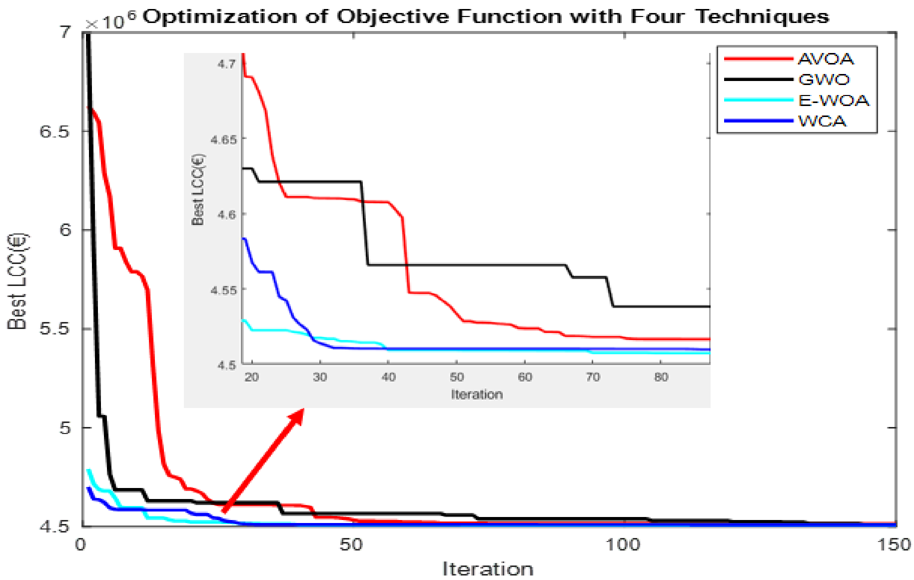

Figure 8. Convergence rates of the AVOA, EWOA, GWOA, and WCA for the optimal cost.

6.3. Discussion on the Application of the Optimal Solution

Table 2 shows the optimal sizes for the system's components based on the EWOA algorithm. These sizes were implemented in the hybrid renewable energy system model. The entire system operated using the derived values for one year, with hourly intervals.

The annual load demand, energy conversion from solar PV, and biogas generation were 9.8664 GWh, 4.0369 GWh, and 4.1435 GWh, respectively. The maximum and minimum values of the power demand, solar PV, and biogas generation were 1.7074 and 0.6682 MW, 2.0484 and 0 MW, and 0.8603 and 0 MW, respectively. Figure 9 displays the annual load demand, the annual output from solar PV, and the biogas power generation.

Figure 10 depicts the annual energy balance, surplus, and deficit in relation to the variation of energy exchanges between the hybrid system and electrical network, considering the pre-defined LPSP values. The figure shows the final energy exchanged with the grid utility, along with the surplus (when the solar PV generation exceeds the load demand and the storage systems (SMES and PHES) are full) and deficit (when the load demand exceeds the generation from the solar PV/biogas system and the PHES upper reservoir water in the tank reaches the minimum allowed level).

The surplus and deficit energy of the hybrid system were about 0.1352 GWh and 0.0281 GWh, respectively, and it reached peak power outputs of 0.876 and 0.19433 MW. The power exchange with the electrical network was equal to the energy surplus sent to the local utility distribution network, varying between the surplus energy and the energy deficit.

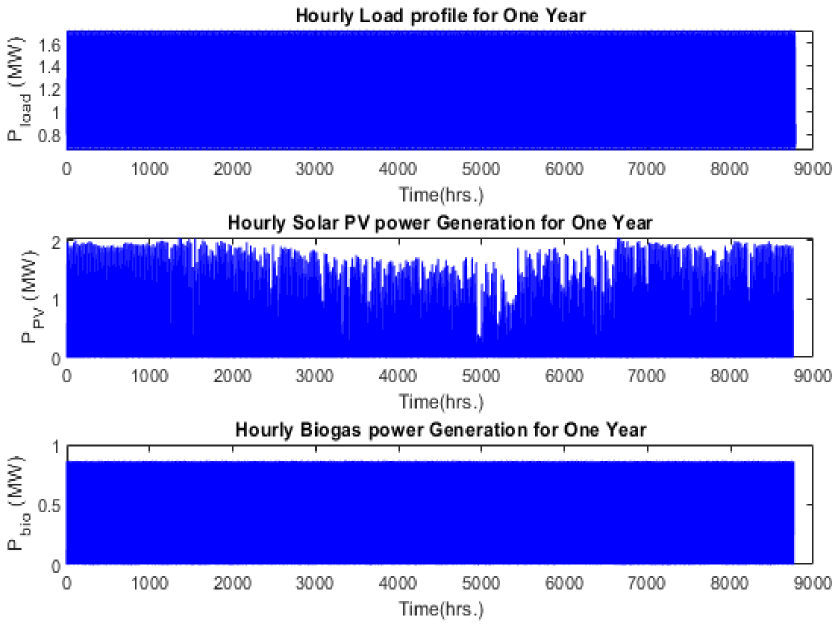

Figure 9. Annual load demand, output power from solar PV, and biogas generation using the EWOA.

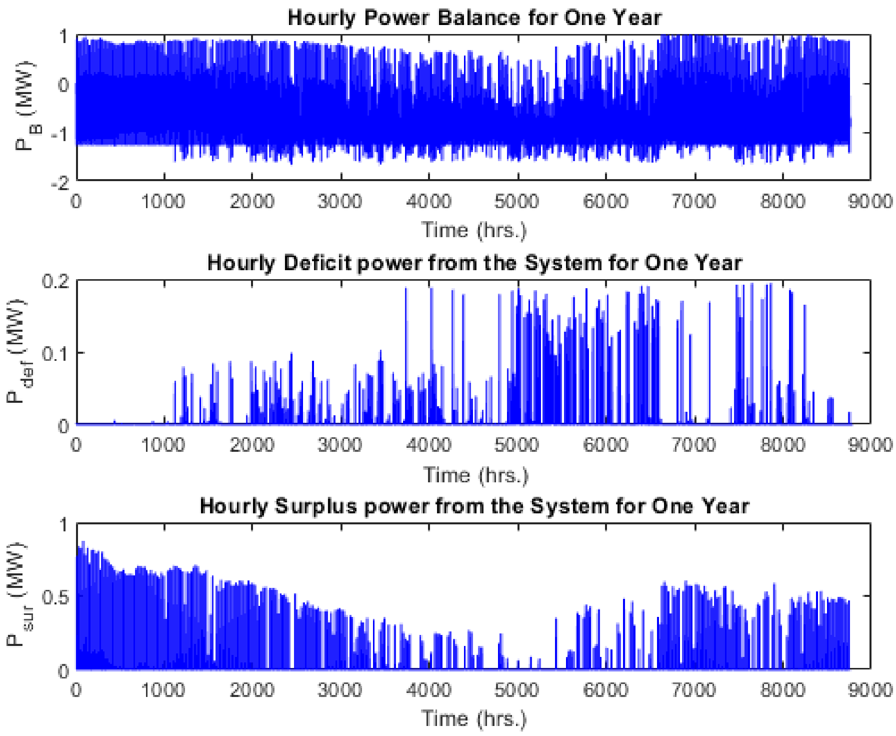

Figure 10. Annual energy balance, deficit, and surplus power from the hybrid system using the EWOA.

Figure 11 presents the continuous changes in discharging power, charging power, and state of charge of the SMES system based on the maximum connected loads. Essentially, this energy storage system performed only during the transition of each energy resource to supply the loads. Since its response time was less than five milliseconds, there was no problem with frequency and power deviation. The annual energy discharge and the charge from/by the SMES system were 0.1236 GWh and 0.1544 GWh. The state of charge of the batteries varied between 5% and 100%.

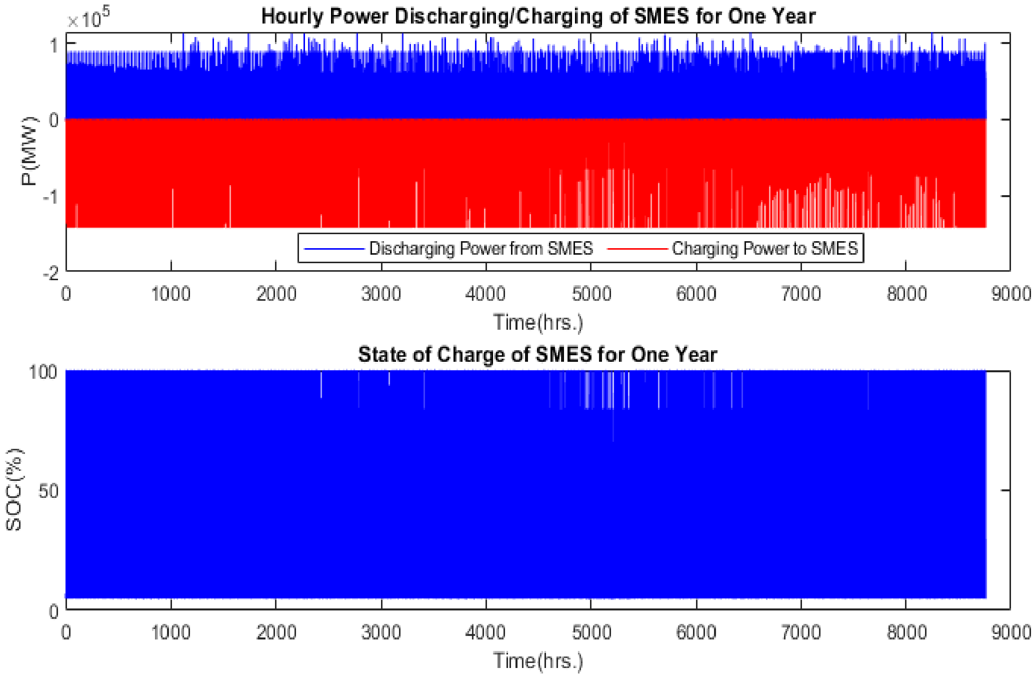

Figure 11. Annual discharging, charging, and SOC representation of the SMES system using the EWOA.

Figure 12 illustrates the consumed energy from solar PV production and the availability of excess power in the proposed hybrid system. This figure represents the PHES energy consumed during charging mode, the PHES energy generated during discharging mode, the amount of water charged to the upper reservoir during pumping mode, the amount of water used/discharged during power generation mode, and the SOC parameter used to control the water level in the upper reservoir. The annual energy consumed/charged and generated/discharged from/by the PHES system was 1.04567 GWh and 0.8667 GWh. The SOC of the upper reservoir indicates the difference between the amounts of water the tank can hold when it is full and when it is empty. The minimum SOC of the upper reservoir was 61%, which was reached during the periods when the PV energy was minimal. The amounts of water annually charged and discharged to/from the PHES upper reservoir were 4.743×10^6 and 4.437×10^6 m^3.

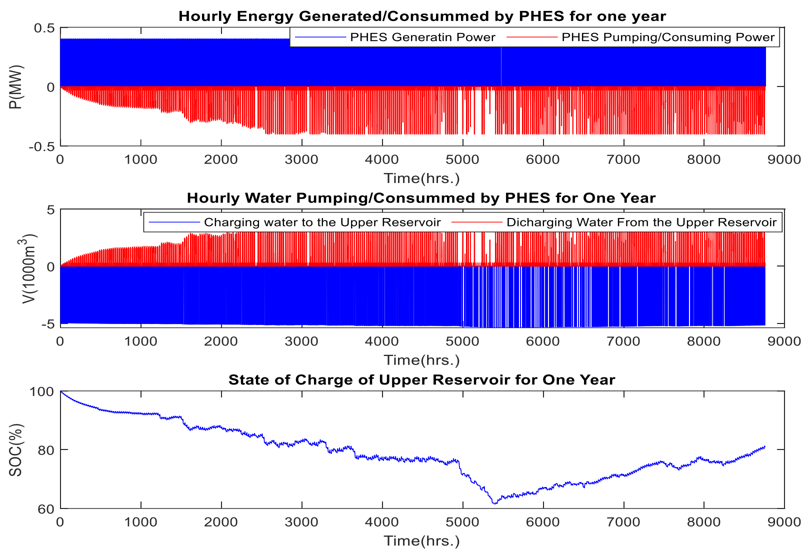

Figure 12. Annual energy consumed and generated, amount of water charged and discharged, and SOC of PHES system using the EWOA.

Figure 13 illustrates the system's 24 h operation for a typical day, which enables the reader to comprehend how the system works. In this figure, two cases ($P_{def.} = 0$ (LPSP = 0%), and $P_{def.} \neq 0$ (LPSP $\neq$ 0% but not greater than 1%)) are illustrated for a typical day.

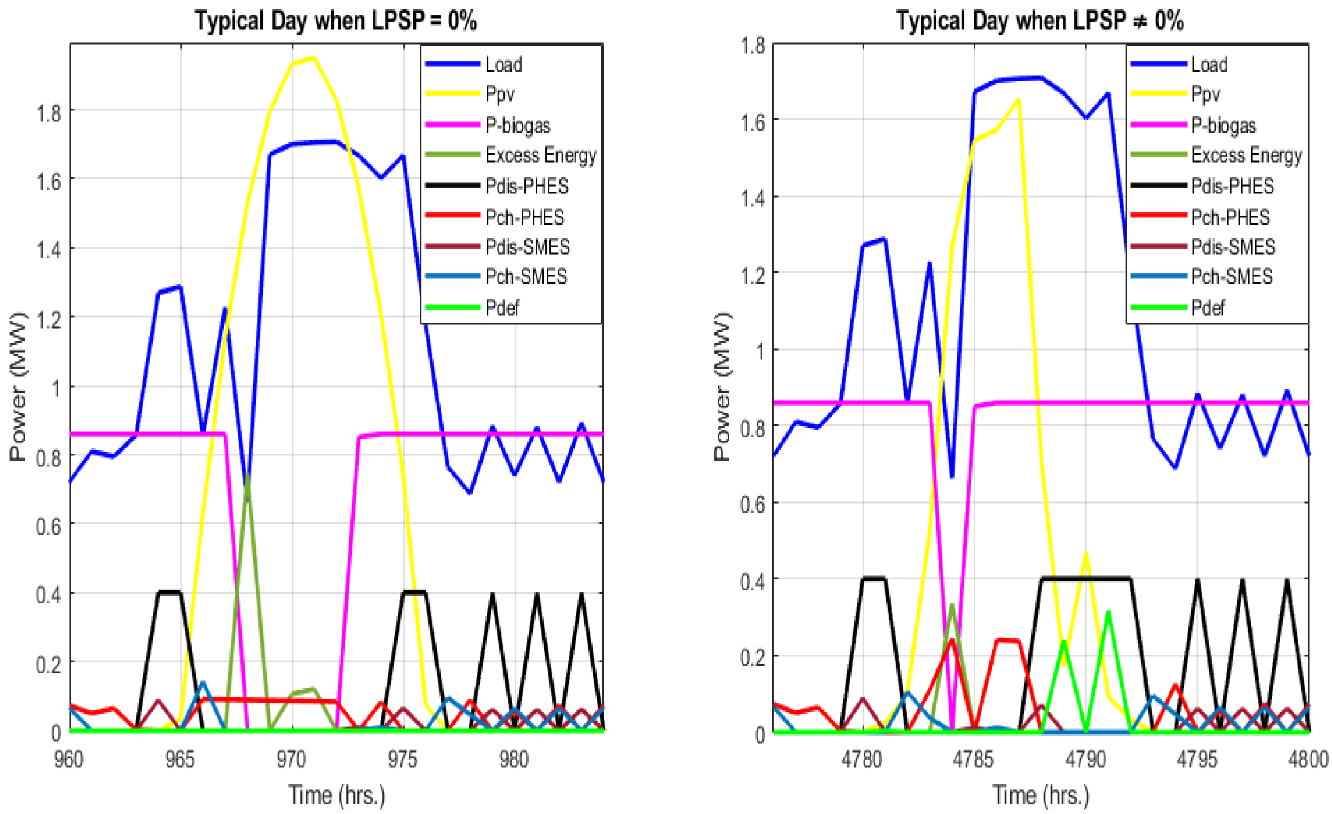

Figure 13. A typical full-day operation based on the results of the EWOA.

7. Conclusions

For the comparative benefits of electric power systems, renewable energy sources (RES), such as photovoltaic (PV), wind, and hydropower systems, have recently begun to replace traditional synchronous power generators. This work investigated the various aspects of replacing backup diesel (since the national grid has more frequent outages) power plants connected to the grid of Debre Markos distribution stations in Ethiopia with renewable energy plants. Based on the selected site's power generation system, a grid-connected hybrid solar/biogas generator with SMES-PHES was proposed to replace the backup diesel power plant. To achieve this, an evaluation of the electrical load demand profile; the solar, biogas, and water resources used for renewable energy; and the sizing of the grid-connected hybrid solar PV/biogas system with SMES-PHES was carried out.

These measures were introduced in an attempt to lower the cost of energy production and increase the reliability of the power system network. The appropriate sizing of the grid-connected hybrid solar PV/biogas generator with SMES-PHES was determined using the EWOA metaheuristic optimization technique. In a detailed design parameter analysis, the capacities of the proposed system's individual components, as well as various types of financial and reliability considerations, were examined. Furthermore, the GWOA, AVOA, and WCA metaheuristic optimization techniques were selected for comparison. After using a MATLAB program to size the hybrid system, LCC values of EUR 4.507×10^6, EUR 4.511×10^6, EUR 4.515×10^6, and EUR 4.509×10^6 were obtained using the EWOA, GWOA, AVOA, and WCA. The LCC estimated by the EWOA for the proposed hybrid system was 1.09%, 1.18%, and 1.05% less than that estimated by the GWOA, AVOA, and WCA, respectively. However, the EWOA reduced the overall LCC in such a way that it remained within the limits of the objective function. The results of the comparison show that the EWOA outperformed the other algorithms in terms of the LCC and reliability indices. Both fast-response (short-term i.e., SMES) storage and long-lasting storage (long-term i.e., PHES) have proven to be efficient in distribution networks.

Author Contributions: Conceptualization, T.F.A., A.F.-L., A.A., I.A., B.K., M.E., W.B.N., O.P.M., R.M.Á. and E.T.; Methodology, T.F.A., A.F.-L., A.A., I.A. and B.K.; Software, T.F.A., A.F.-L., A.A., B.K., M.E., W.B.N., O.P.M. and E.T.; Validation, T.F.A., A.F.-L., A.A., I.A., B.K., O.P.M. and R.M.Á.; Formal analysis, T.F.A., A.F.-L., A.A., I.A., B.K., M.E., W.B.N. and E.T.; Investigation, T.F.A., A.F.-L., A.A., I.A., B.K., M.E., O.P.M., R.M.Á. and E.T.; Resources, T.F.A., A.F.-L., A.A., I.A., B.K., W.B.N., O.P.M. and E.T.; Data curation, T.F.A., A.F.-L., A.A., I.A., B.K., M.E. and E.T.; Writing—original draft, T.F.A., A.F.-L., A.A., I.A., B.K. and O.P.M.; Writing—review & editing, T.F.A., A.F.-L., I.A., B.K., M.E., W.B.N., O.P.M., R.M.Á. and E.T.; Visualization, T.F.A., A.F.-L., A.A., I.A., B.K., M.E., O.P.M., R.M.Á. and E.T.; Supervision, A.F.-L., A.A., B.K., W.B.N., O.P.M., R.M.Á. and E.T.; Project administration, T.F.A. All authors have read and agreed to the published version of the manuscript.

Funding: This research received no external funding.

Institutional Review Board Statement: Not applicable.

Informed Consent Statement: Not applicable.

Data Availability Statement: The data presented in this study are available on request from the corresponding author.

Acknowledgments: The authors kindly thank the Editor and reviewers who spent their valuable time to improve the present paper. Takele Ferede Agajie kindly thanks the financial support of the MIRET Scholarship program through project No.: 614658-PANAF-1-2019-1-KE-PANAF-MOBAF.

Conflicts of Interest: The authors declare no conflict of interest.

References

1. Tan, Q.; Wen, X.; Sun, Y.; Lei, X.; Wang, Z.; Qin, G. Evaluation of the risk and benefit of the complementary operation of the large wind-photovoltaic-hydropower system considering forecast uncertainty. *Appl. Energy* **2021**, *285*, 116442. [CrossRef]
2. Zhong, J.; Bollen, M.; Rönnberg, S. Towards a 100% renewable energy electricity generation system in Sweden. *Renew. Energy* **2021**, *171*, 812–824. [CrossRef]
3. Guzović, Z.; Duic, N.; Piacentino, A.; Markovska, N.; Mathiesen, B.V.; Lund, H. Recent advances in methods, policies and technologies at sustainable energy systems development. *Energy* **2022**, *245*, 123276. [CrossRef]
4. Samour, A.; Baskaya, M.M.; Tursoy, T. The impact of financial development and FDI on renewable energy in the UAE: A path towards sustainable development. *Sustainability* **2022**, *14*, 1208. [CrossRef]
5. Yoro, K.O.; Daramola, M.O. Chapter 1—CO_2 emission sources, greenhouse gases, and the global warming effect. In *Advances in Carbon Capture*; Rahimpour, M.R., Farsi, M., Makarem, M.A., Eds.; Woodhead Publishing: Sawston, UK, 2020; pp. 3–28. [CrossRef]
6. Du, Y.; Gao, T.; Rochelle, G.T.; Bhown, A.S. Zero- and negative-emissions fossil-fired power plants using CO_2 capture by conventional aqueous amines. *Int. J. Greenh. Gas Control* **2021**, *111*, 103473. [CrossRef]
7. Mostafaeipour, A.; Bidokhti, A.; Fakhrzad, M.-B.; Sadegheih, A.; Mehrjerdi, Y.Z. A new model for the use of renewable electricity to reduce carbon dioxide emissions. *Energy* **2022**, *238*, 121602. [CrossRef]
8. Cho, H.H.; Strezov, V. A Comparative Review on the Environmental Impacts of Combustion-Based Electricity Generation Technologies. *Energy Fuels* **2020**, *34*, 10486–10502. [CrossRef]
9. Child, M.; Kemfert, C.; Bogdanov, D.; Breyer, C. Flexible electricity generation, grid exchange and storage for the transition to a 100% renewable energy system in Europe. *Renew. Energy* **2019**, *139*, 80–101. [CrossRef]
10. Al-Shetwi, A.Q.; Hannan, M.A.; Jern, K.P.; Mansur, M.; Mahlia, T.M.I. Grid-connected renewable energy sources: Review of the recent integration requirements and control methods. *J. Clean. Prod.* **2020**, *253*, 119831. [CrossRef]
11. Ayamolowo, O.J.; Manditereza, P.; Kusakana, K. Exploring the gaps in renewable energy integration to grid. *Energy Rep.* **2020**, *6*, 992–999. [CrossRef]
12. Deng, X.; Lv, T. Power system planning with increasing variable renewable energy: A review of optimization models. *J. Clean. Prod.* **2020**, *246*, 118962. [CrossRef]
13. Coester, A.; Hofkes, M.W.; Papyrakis, E. An optimal mix of conventional power systems in the presence of renewable energy: A new design for the German electricity market. *Energy Policy* **2018**, *116*, 312–322. [CrossRef]
14. Adewumi, O.B.; Fotis, G.; Vita, V.; Nankoo, D.; Ekonomou, L. The Impact of Distributed Energy Storage on Distribution and Transmission Networks' Power Quality. *Appl. Sci.* **2022**, *12*, 6466. [CrossRef]

15. Shin, W.; Lee, C.; Chung, I.-Y.; Lim, J.; Youn, J.; Rhie, Y.; Hur, K.; Shim, J.W. Reserve replacement from governor to energy storage system on conventional generator for operating-cost reduction. *Appl. Energy* **2022**, *324*, 119697. [CrossRef]
16. Choudhury, S. Flywheel energy storage systems: A critical review on technologies, applications, and future prospects. *Int. Trans. Electr. Energy Syst.* **2021**, *31*, e13024. [CrossRef]
17. Kumar, G.B.; Palanisamy, K. Review of Energy Storage System for Microgrid. *Microgrid Technol.* **2021**, 57–90. [CrossRef]
18. Zyryanov, V.; Kiryanova, N.; Korotkov, I.; Nesterenko, G.; Prankevich, G.; Rudiuk, I. Analysis of energy storage systems application in the Russian and world electric power industry. In Proceedings of the 2020 Ural Smart Energy Conference (USEC), Ekaterinburg, Russia, 13–15 November 2020; pp. 106–109.
19. Koohi-Fayegh, S.; Rosen, M.A. A review of energy storage types, applications and recent developments. *J. Energy Storage* **2020**, *27*, 101047. [CrossRef]
20. Matos, C.R.; Carneiro, J.F.; Silva, P.P. Overview of large-scale underground energy storage technologies for integration of renewable energies and criteria for reservoir identification. *J. Energy Storage* **2018**, *21*, 241–258. [CrossRef]
21. Blakers, A.; Stocks, M.; Lu, B.; Cheng, C. A review of pumped hydro energy storage. *Prog. Energy* **2021**, *3*, 022003. [CrossRef]
22. Olabi, A.; Wilberforce, T.; Ramadan, M.; Abdelkareem, M.A.; Alami, A.H. Compressed air energy storage systems: Components and operating parameters—A review. *J. Energy Storage* **2021**, *34*, 102000. [CrossRef]
23. Olabi, A.G.; Wilberforce, T.; Abdelkareem, M.A.; Ramadan, M. Critical Review of Flywheel Energy Storage System. *Energies* **2021**, *14*, 2159. [CrossRef]
24. Ali, M.; Sarker, M.R.; Saad, M.H.M.; Mohamed, R. Overview of Control System Topology of Flywheel Energy Storage System in Renewable Energy Application for Alternative Power Plant. *Przegląd Elektrotechniczny* **2022**, *1*, 147–155. [CrossRef]
25. Olabi, A.G.; Abbas, Q.; Al Makky, A.; Abdelkareem, M.A. Supercapacitors as next generation energy storage devices: Properties and applications. *Energy* **2022**, *248*, 123617. [CrossRef]
26. Colmenar-Santos, A.; Molina-Ibáñez, E.-L.; Rosales-Asensio, E.; López-Rey, Á. Technical approach for the inclusion of superconducting magnetic energy storage in a smart city. *Energy* **2018**, *158*, 1080–1091. [CrossRef]
27. Jiao, Y.; Månsson, D. A Study of the Energy Exchange within a Hybrid Energy Storage System and a Comparison of the Capacities, Lifetimes, and Costs of Different Systems. *Energies* **2021**, *14*, 7045. [CrossRef]
28. Hajiaghasi, S.; Salemnia, A.; Hamzeh, M. Hybrid energy storage system for microgrids applications: A review. *J. Energy Storage* **2019**, *21*, 543–570. [CrossRef]
29. Tabart, Q.; Vechiu, I.; Etxeberria, A.; Bacha, S. Hybrid Energy Storage System Microgrids Integration for Power Quality Improvement Using Four-Leg Three-Level NPC Inverter and Second-Order Sliding Mode Control. *IEEE Trans. Ind. Electron.* **2017**, *65*, 424–435. [CrossRef]
30. Geetha, A.; Subramani, C. A comprehensive review on energy management strategies of hybrid energy storage system for electric vehicles. *Int. J. Energy Res.* **2017**, *41*, 1817–1834. [CrossRef]
31. Kasimalla, V.K.; Velisala, V. A review on energy allocation of fuel cell/battery/ultracapacitor for hybrid electric vehicles. *Int. J. Energy Res.* **2018**, *42*, 4263–4283. [CrossRef]
32. Wieczorek, M.; Lewandowski, M. A mathematical representation of an energy management strategy for hybrid energy storage system in electric vehicle and real time optimization using a genetic algorithm. *Appl. Energy* **2017**, *192*, 222–233. [CrossRef]
33. Hemmati, R.; Saboori, H. Emergence of hybrid energy storage systems in renewable energy and transport applications—A review. *Renew. Sustain. Energy Rev.* **2016**, *65*, 11–23. [CrossRef]
34. Sutikno, T.; Arsadiando, W.; Wangsupphaphol, A.; Yudhana, A.; Facta, M. A review of recent advances on hybrid energy storage system for solar photovoltaics power generation. *IEEE Access* **2022**, *10*, 42346–42364. [CrossRef]
35. Ramadan, H.S.; Alhelou, H.H.; Ahmed, A.A. Impartial near-optimal control and sizing for battery hybrid energy system balance via grey wolf optimizers: Lead acid and lithium-ion technologies. *IET Renew. Power Gener.* **2022**, 1–14. [CrossRef]
36. Tahir, Y.; Nadeem, M.F.; Ahmed, A.; Khan, I.A.; Qamar, F. A Review on Hybrid Energy Storage Systems in Microgrids. In Proceedings of the 2020 3rd International Conference on Computing, Mathematics and Engineering Technologies (iCoMET), Sukkur, Pakistan, 29–30 January 2020; pp. 1–7. [CrossRef]
37. Ibrahim, H.; Rezkallah, M.; Ilinca, A.; Ghandour, M. 10—Hybrid energy storage systems. In *Hybrid Renewable Energy Systems and Microgrids*; Kabalci, E., Ed.; Academic Press: Cambridge, MA, USA, 2021; pp. 351–372. [CrossRef]
38. Rohit, A.K.; Rangnekar, S. An overview of energy storage and its importance in Indian renewable energy sector: Part II–energy storage applications, benefits and market potential. *J. Energy Storage* **2017**, *13*, 447–456. [CrossRef]
39. Li, J.; Yang, Q.; Yao, P.; Sun, Q.; Zhang, Z.; Zhang, M.; Yuan, W. A Novel use of the Hybrid Energy Storage System for Primary Frequency Control in a Microgrid. *Energy Procedia* **2016**, *103*, 82–87. [CrossRef]
40. Li, J.; Xiong, R.; Yang, Q.; Liang, F.; Zhang, M.; Yuan, W. Design/test of a hybrid energy storage system for primary frequency control using a dynamic droop method in an isolated microgrid power system. *Appl. Energy* **2017**, *201*, 257–269. [CrossRef]
41. Althubaiti, M.; Bernard, M.; Musilek, P. Fuzzy logic controller for hybrid renewable energy system with multiple types of storage. In Proceedings of the 2017 IEEE 30th Canadian Conference on Electrical and Computer Engineering (CCECE), Windsor, ON, Canada, 30 April–3 May 2017; pp. 1–6. [CrossRef]
42. Martín, I.S.; Ursua, A.; Sanchis, P. Integration of fuel cells and supercapacitors in electrical microgrids: Analysis, modelling and experimental validation. *Int. J. Hydrogen Energy* **2013**, *38*, 11655–11671. [CrossRef]

43. Guney, M.S.; Tepe, Y. Classification and assessment of energy storage systems. *Renew. Sustain. Energy Rev.* **2017**, *75*, 1187–1197. [CrossRef]
44. Arani, A.K.; Karami, H.; Gharehpetian, G.; Hejazi, M. Review of Flywheel Energy Storage Systems structures and applications in power systems and microgrids. *Renew. Sustain. Energy Rev.* **2017**, *69*, 9–18. [CrossRef]
45. Inthamoussou, F.A.; Pegueroles-Queralt, J.; Bianchi, F.D. Control of a supercapacitor energy storage system for microgrid applications. *IEEE Trans. Energy Convers.* **2013**, *28*, 690–697. [CrossRef]
46. Faisal, M.; Hannan, M.A.; Ker, P.J.; Hussain, A.; Mansor, M.B.; Blaabjerg, F. Review of energy storage system technologies in microgrid applications: Issues and challenges. *IEEE Access* **2018**, *6*, 35143–35164. [CrossRef]
47. Reza, M.S.; Rahman, N.; Wali, S.B.; Hannan, M.A.; Ker, P.J.; Rahman, S.A.; Muttaqi, K.M. Optimal Algorithms for Energy Storage Systems in Microgrid Applications: An Analytical Evaluation Towards Future Directions. *IEEE Access* **2022**, *10*, 10105–10123. [CrossRef]
48. Elfeky, K.E.; Mohammed, A.G.; Wang, Q. Thermal Performance Evaluation of Combined Sensible-Latent Heat Storage Tank with a Different Storage Medium. *Chem. Eng. Trans.* **2022**, *94*, 1267–1272. [CrossRef]
49. Li, G.; Lu, X.; Kim, J.Y.; Meinhardt, K.D.; Chang, H.J.; Canfield, N.L.; Sprenkle, V.L. Advanced intermediate temperature sodium–nickel chloride batteries with ultra-high energy density. *Nat. Commun.* **2016**, *7*, 10683. [CrossRef]
50. Karimi-Rizvandi, A.; Sandjareh, M.B.; Nazari, M.H.; Ezati-Yaraziz, M. A Novel Frequency Control Scheme for Autonomous Microgrid Using Cooperative Application of Supercapacitor-Battery HESS, Photovoltaics, LED Lighting Loads and TCLs. *IEEE Access* **2021**, *9*, 57198–57214. [CrossRef]
51. Song, Z.; Li, J.; Han, X.; Xu, L.; Lu, L.; Ouyang, M.; Hofmann, H. Multi-objective optimization of a semi-active battery/supercapacitor energy storage system for electric vehicles. *Appl. Energy* **2014**, *135*, 212–224. [CrossRef]
52. Jing, W.; Lai, C.H.; Wong, W.S.; Wong, M.D. Dynamic power allocation of battery-supercapacitor hybrid energy storage for standalone PV microgrid applications. *Sustain. Energy Technol. Assess.* **2017**, *22*, 55–64. [CrossRef]
53. Yuan, Y.; Sun, C.; Li, M.; Choi, S.S.; Li, Q. Determination of optimal supercapacitor-lead-acid battery energy storage capacity for smoothing wind power using empirical mode decomposition and neural network. *Electr. Power Syst. Res.* **2015**, *127*, 323–331. [CrossRef]
54. Chen, L.; Chen, H.; Li, Y.; Li, G.; Yang, J.; Liu, X.; Xu, Y.; Ren, L.; Tang, Y. SMES-Battery Energy Storage System for the Stabilization of a Photovoltaic-Based Microgrid. *IEEE Trans. Appl. Supercond.* **2018**, *28*, 1–7. [CrossRef]
55. Cansiz, A.; Faydaci, C.; Qureshi, M.T.; Usta, O.; McGuiness, D.T. Integration of a SMES–Battery-Based Hybrid Energy Storage System into Microgrids. *J. Supercond. Nov. Magn.* **2018**, *31*, 1449–1457. [CrossRef]
56. Ding, K.; Li, W.; Hu, P.; Hu, A.; Tao, Y.; Zhuang, J.; Lu, H. The Voltage Sag Mitigation Method Based on Hybrid SMES-BES Dynamic Voltage Restorer (DVR). In Proceedings of the 2019 IEEE 3rd International Electrical and Energy Conference (CIEEC), Beijing, China, 7–9 September 2019; pp. 545–549. [CrossRef]
57. Abbassi, A.; Dami, M.A.; Jemli, M. Statistical characterization of capacity of Hybrid Energy Storage System (HESS) to assimilate the fast PV-Wind power generation fluctuations. In Proceedings of the 2017 International Conference on Advanced Systems and Electric Technologies (IC_ASET), Hammamet, Tunisia, 14–17 January 2017; pp. 467–472. [CrossRef]
58. Ma, W.; Wang, W.; Wu, X.; Hu, R.; Tang, F.; Zhang, W.; Han, X.; Ding, L. Optimal Allocation of Hybrid Energy Storage Systems for Smoothing Photovoltaic Power Fluctuations Considering the Active Power Curtailment of Photovoltaic. *IEEE Access* **2019**, *7*, 74787–74799. [CrossRef]
59. Ma, T.; Yang, H.; Lu, L. Development of hybrid battery–supercapacitor energy storage for remote area renewable energy systems. *Appl. Energy* **2015**, *153*, 56–62. [CrossRef]
60. Wang, S.; Tang, Y.; Shi, J.; Gong, K.; Liu, Y.; Ren, L.; Li, J. Design and advanced control strategies of a hybrid energy storage system for the grid integration of wind power generations. *IET Renew. Power Gener.* **2015**, *9*, 89–98. [CrossRef]
61. Lamsal, D.; Sreeram, V.; Mishra, Y.; Kumar, D. Output power smoothing control approaches for wind and photovoltaic generation systems: A review. *Renew. Sustain. Energy Rev.* **2019**, *113*, 109245. [CrossRef]
62. Talal, M.; Kaddah, S.S.; Eladl, A.A. Impact of Energy Storage Devices on the Distribution System Stability with Distributed Generation. *MEJ Mansoura Eng. J.* **2020**, *45*, 1–10. [CrossRef]
63. Li, J.; Yang, Q.; Robinson, F.; Liang, F.; Zhang, M.; Yuan, W. Design and test of a new droop control algorithm for a SMES/battery hybrid energy storage system. *Energy* **2017**, *118*, 1110–1122. [CrossRef]
64. Yuan, X.; Song, C.; Platt, A.; Zhao, N.; Wang, H.; Li, H.; Fatih, K.; Jang, D. A review of all-vanadium redox flow battery durability: Degradation mechanisms and mitigation strategies. *Int. J. Energy Res.* **2019**, *43*, 6599–6638. [CrossRef]
65. Shchurov, N.I.; Dedov, S.I.; Malozyomov, B.V.; Shtang, A.A.; Martyushev, N.V.; Klyuev, R.V.; Andriashin, S.N. Degradation of Lithium-Ion Batteries in an Electric Transport Complex. *Energies* **2021**, *14*, 8072. [CrossRef]
66. Zdiri, M.A.; Guesmi, T.; Alshammari, B.M.; Alqunun, K.; Almalaq, A.; Ben Salem, F.; Abdallah, H.H.; Toumi, A. Design and Analysis of Sliding-Mode Artificial Neural Network Control Strategy for Hybrid PV-Battery-Supercapacitor System. *Energies* **2022**, *15*, 4099. [CrossRef]
67. Babu, T.S.; Vasudevan, K.R.; Ramachandaramurthy, V.K.; Sani, S.B.; Chemud, S.; Lajim, R.M. A comprehensive review of hybrid energy storage systems: Converter topologies, control strategies and future prospects. *IEEE Access* **2020**, *8*, 148702–148721. [CrossRef]

68. Faria, J.; Pombo, J.; Calado, M.d.R.; Mariano, S. Power Management Control Strategy Based on Artificial Neural Networks for Standalone PV Applications with a Hybrid Energy Storage System. *Energies* **2019**, *12*, 902. [CrossRef]
69. Li, J.; Zhang, M.; Yang, Q.; Zhang, Z.; Yuan, W. SMES/Battery Hybrid Energy Storage System for Electric Buses. *IEEE Trans. Appl. Supercond.* **2016**, *26*, 1–5. [CrossRef]
70. Barelli, L.; Bidini, G.; Ciupageanu, D.; Pelosi, D. Integrating Hybrid Energy Storage System on a Wind Generator to enhance grid safety and stability: A Levelized Cost of Electricity analysis. *J. Energy Storage* **2021**, *34*, 102050. [CrossRef]
71. Qi, M.; Liu, Y.; Landon, R.S.; Liu, Y.; Moon, I. Assessing and mitigating potential hazards of emerging grid-scale electrical energy storage systems. *Process Saf. Environ. Prot.* **2021**, *149*, 994–1016. [CrossRef]
72. Barelli, L.; Bidini, G.; Cherubini, P.; Micangeli, A.; Pelosi, D.; Tacconelli, C. How Hybridization of Energy Storage Technologies Can Provide Additional Flexibility and Competitiveness to Microgrids in the Context of Developing Countries. *Energies* **2019**, *12*, 3138. [CrossRef]
73. Lawder, M.T.; Suthar, B.; Northrop, P.W.C.; DE, S.; Hoff, C.M.; Leitermann, O.; Crow, M.L.; Santhanagopalan, S.; Subramanian, V.R. Battery Energy Storage System (BESS) and Battery Management System (BMS) for Grid-Scale Applications. *Proc. IEEE* **2014**, *102*, 1014–1030. [CrossRef]
74. Ogunniyi, E.O.; Pienaar, H. Overview of battery energy storage system advancement for renewable (photovoltaic) energy applications. In Proceedings of the 2017 International Conference on the Domestic Use of Energy (DUE), Cape Town, South Africa, 4–5 April 2017; pp. 233–239.
75. Alami, A.H.; Yasin, A.; Alrashid, R.; Alasad, S.; Aljaghoub, H.; Alabsi, G.; Alketbi, L.; Alkhzaimi, A.; Alteneji, A.; Shikhli, S. Experimental evaluation of compressed air energy storage as a potential replacement of electrochemical batteries. *J. Energy Storage* **2022**, *54*, 105263. [CrossRef]
76. Ghadi, M.J.; Azizivahed, A.; Mishra, D.K.; Li, L.; Zhang, J.; Shafie-Khah, M.; Catalão, J.P. Application of small-scale compressed air energy storage in the daily operation of an active distribution system. *Energy* **2021**, *231*, 120961. [CrossRef]
77. Yang, D.; Wang, M.; Yang, R.; Zheng, Y.; Pandzic, H. Optimal dispatching of an energy system with integrated compressed air energy storage and demand response. *Energy* **2021**, *234*, 121232. [CrossRef]
78. Ali, M.H.; Wu, B.; Dougal, R.A. An Overview of SMES Applications in Power and Energy Systems. *IEEE Trans. Sustain. Energy* **2010**, *1*, 38–47. [CrossRef]
79. Amaro, N.; Pina, J.M.; Martins, J.; Ceballos, J.M. Amaro, N.; Pina, J.M.; Martins, J.; Ceballos, J.M. A Study on Superconducting Coils for Superconducting Magnetic Energy Storage (SMES) Applications. In *Technological Innovation for the Internet of Things*; Springer: Berlin/Heidelberg, Germany, 2013; pp. 449–456. [CrossRef]
80. Al Zaman, A.; Islam, M.; Maruf, H. Study on Conceptual Designs of Superconducting Coil for Energy Storage in SMES. *East Eur. J. Phys.* **2020**, 111–120. [CrossRef]
81. Moghadasi, A.H.; Heydari, H.; Farhadi, M. Pareto Optimality for the Design of SMES Solenoid Coils Verified by Magnetic Field Analysis. *IEEE Trans. Appl. Supercond.* **2010**, *21*, 13–20. [CrossRef]
82. Li, J.; Gee, A.M.; Zhang, M.; Yuan, W. Analysis of battery lifetime extension in a SMES-battery hybrid energy storage system using a novel battery lifetime model. *Energy* **2015**, *86*, 175–185. [CrossRef]
83. Mohamad, F.; Teh, J.; Lai, C.-M.; Chen, L.-R. Development of Energy Storage Systems for Power Network Reliability: A Review. *Energies* **2018**, *11*, 2278. [CrossRef]
84. Hannan, M.; Faisal, M.; Ker, P.J.; Begum, R.; Dong, Z.; Zhang, C. Review of optimal methods and algorithms for sizing energy storage systems to achieve decarbonization in microgrid applications. *Renew. Sustain. Energy Rev.* **2020**, *131*, 110022. [CrossRef]
85. Xu, Y.; Li, Y.; Ren, L.; Xu, C.; Tang, Y.; Li, J.; Chen, L.; Jia, B. Research on the Application of Superconducting Magnetic Energy Storage in Microgrids for Smoothing Power Fluctuation Caused by Operation Mode Switching. *IEEE Trans. Appl. Supercond.* **2018**, *28*, 1–6. [CrossRef]
86. Kularatna, N.; Jayananda, D. Supercapacitor-Based Long Time-Constant Circuits: A Unique Design Opportunity for New Power Electronic Circuit Topologies. *IEEE Ind. Electron. Mag.* **2020**, *14*, 40–56. [CrossRef]
87. Ren, G.; Ma, G.; Cong, N. Review of electrical energy storage system for vehicular applications. *Renew. Sustain. Energy Rev.* **2015**, *41*, 225–236. [CrossRef]
88. Ma, T.; Yang, H.; Lu, L. Feasibility study and economic analysis of pumped hydro storage and battery storage for a renewable energy powered island. *Energy Convers. Manag.* **2014**, *79*, 387–397. [CrossRef]
89. Ma, T.; Yang, H.; Lu, L.; Peng, J. Technical feasibility study on a standalone hybrid solar-wind system with pumped hydro storage for a remote island in Hong Kong. *Renew. Energy* **2014**, *69*, 7–15. [CrossRef]
90. Ma, T.; Yang, H.; Lu, L.; Peng, J. Optimal design of an autonomous solar–wind-pumped storage power supply system. *Appl. Energy* **2015**, *160*, 728–736. [CrossRef]
91. Ma, T.; Yang, H.; Lu, L.; Peng, J. Pumped storage-based standalone photovoltaic power generation system: Modeling and techno-economic optimization. *Appl. Energy* **2015**, *137*, 649–659. [CrossRef]
92. Vijay, R.; Sowmya, R. Optimal sitting of PV-wind-energy storage system integrated micro grid using artificial bee colony optimization technique. *Int. J. Innov. Res. Comput. Commun. Eng.* **2017**, *80*, 9640–9652.
93. Khosravi, M.; Afsharnia, S.; Farhangi, S. Optimal sizing and technology selection of hybrid energy storage system with novel dispatching power for wind power integration. *Int. J. Electr. Power Energy Syst.* **2021**, *127*, 106660. [CrossRef]

94. Zhou, T.; Sun, W. Optimization of Battery–Supercapacitor Hybrid Energy Storage Station in Wind/Solar Generation System. *IEEE Trans. Sustain. Energy* **2014**, *5*, 408–415. [CrossRef]
95. Hailu, A.; Mezgebu, C. Design and simulation of standalone hybrid (solar/biomass) electricity generation system for a rural village in Ethiopia. *Int. J. Sci. Eng. Res.* **2017**, *8*, 1570–1574.
96. Kefalew, T.; Lami, M. Biogas and bio-fertilizer production potential of abattoir waste: Implication in sustainable waste management in Shashemene City, Ethiopia. *Heliyon* **2021**, *7*, e08293. [CrossRef]
97. Leung, D.Y.C.; Wang, J. An overview on biogas generation from anaerobic digestion of food waste. *Int. J. Green Energy* **2016**, *13*, 119–131. [CrossRef]
98. Anand, P.; Rizwan, M.; Bath, S.K. Sizing of renewable energy based hybrid system for rural electrification using grey wolf optimisation approach. *IET Energy Syst. Integr.* **2019**, *1*, 158–172. [CrossRef]
99. Yaghoubi, M.; Eslami, M.; Noroozi, M.; Mohammadi, H.; Kamari, O.; Palani, S. Modified Salp Swarm Optimization for Parameter Estimation of Solar PV Models. *IEEE Access* **2022**, *10*, 110181–110194. [CrossRef]
100. Diab, A.A.Z.; El-ajmi, S.I.; Sultan, H.M.; Hassan, Y.B. Modified farmland fertility optimization algorithm for optimal design of a grid-connected hybrid renewable energy system with fuel cell storage: Case study of Ataka, Egypt. *Int. J. Adv. Comput. Sci. Appl.* **2019**, *10*, 119–132. [CrossRef]
101. Heydari, A.; Askarzadeh, A. Optimization of a biomass-based photovoltaic power plant for an off-grid application subject to loss of power supply probability concept. *Appl. Energy* **2016**, *165*, 601–611. [CrossRef]
102. Rehman, S.; Al-Hadhrami, L.M.; Alam, M.M. Pumped hydro energy storage system: A technological review. *Renew. Sustain. Energy Rev.* **2015**, *44*, 586–598. [CrossRef]
103. Molina, M.G.; Mercado, P.E.; Watanabe, E.H. Improved Superconducting Magnetic Energy Storage (SMES) Controller for High-Power Utility Applications. *IEEE Trans. Energy Convers.* **2011**, *26*, 444–456. [CrossRef]
104. Alhamali, A.; Farrag, M.E.; Bevan, G.; Hepburn, D.M. Review of Energy Storage Systems in electric grid and their potential in distribution networks. In Proceedings of the 2016 Eighteenth International Middle East Power Systems Conference (MEPCON), Cairo, Egypt, 27–29 December 2016; pp. 546–551. [CrossRef]
105. Worku, M.Y. Recent Advances in Energy Storage Systems for Renewable Source Grid Integration: A Comprehensive Review. *Sustainability* **2022**, *14*, 5985. [CrossRef]
106. Pappachen, A.; Fathima, A.P. Critical research areas on load frequency control issues in a deregulated power system: A state-of-the-art-of-review. *Renew. Sustain. Energy Rev.* **2017**, *72*, 163–177. [CrossRef]
107. Mir, A.S.; Senroy, N. Adaptive Model Predictive Control Scheme for Application of SMES for Load Frequency Control. *IEEE Trans. Power Syst.* **2017**, 1. [CrossRef]
108. Shayeghi, H.; Shayanfar, H.; Jalili, A. Load frequency control strategies: A state-of-the-art survey for the researcher. *Energy Convers. Manag.* **2009**, *50*, 344–353. [CrossRef]
109. Deng, J.; Shi, J.; Liu, Y.; Tang, Y. Application of a hybrid energy storage system in the fast charging station of electric vehicles. *IET Gener. Transm. Distrib.* **2016**, *10*, 1092–1097. [CrossRef]
110. Gupta, S.; Kumar, Y.; Agnihotri, G. Design of an autonomous renewable hybrid power system. *Int. J. Renew. Energy Technol.* **2011**, *2*, 86. [CrossRef]
111. Salman, U.T.; Al-Ismail, F.S.; Khalid, M. Optimal Sizing of Battery Energy Storage for Grid-Connected and Isolated Wind-Penetrated Microgrid. *IEEE Access* **2020**, *8*, 91129–91138. [CrossRef]
112. Borhanazad, H.; Mekhilef, S.; Ganapathy, V.G.; Modiri-Delshad, M.; Mirtaheri, A. Optimization of micro-grid system using MOPSO. *Renew. Energy* **2014**, *71*, 295–306. [CrossRef]
113. Bukar, A.L.; Tan, C.W.; Lau, K.Y. Optimal sizing of an autonomous photovoltaic/wind/battery/diesel generator microgrid using grasshopper optimization algorithm. *Sol. Energy* **2019**, *188*, 685–696. [CrossRef]
114. Zhou, T.; Francois, B. Energy Management and Power Control of a Hybrid Active Wind Generator for Distributed Power Generation and Grid Integration. *IEEE Trans. Ind. Electron.* **2011**, *58*, 95–104. [CrossRef]
115. Ramli, M.A.; Bouchekara, H.; Alghamdi, A.S. Optimal sizing of PV/wind/diesel hybrid microgrid system using multi-objective self-adaptive differential evolution algorithm. *Renew. Energy* **2018**, *121*, 400–411. [CrossRef]
116. El-Sattar, H.A.; Sultan, H.M.; Kamel, S.; Menesy, A.S.; Rahmann, C. Optimal Design of Hybrid Stand-alone Microgrids Using Tunicate Swarm Algorithm. In Proceedings of the 2021 IEEE International Conference on Automation/XXIV Congress of the Chilean Association of Automatic Control (ICA-ACCA), Online, 22–26 March 2021; pp. 1–6. [CrossRef]
117. Abu-Rumman, A.K.; Muslih, I.; Barghash, M.A. Life Cycle Costing of PV Generation System. *J. Appl. Res. Ind. Eng.* **2017**, *4*, 252–258. [CrossRef]
118. Munuswamy, S.; Nakamura, K.; Katta, A. Comparing the cost of electricity sourced from a fuel cell-based renewable energy system and the national grid to electrify a rural health centre in India: A case study. *Renew. Energy* **2011**, *36*, 2978–2983. [CrossRef]
119. Diaf, S.; Notton, G.; Belhamel, M.; Haddadi, M.; Louche, A. Design and techno-economical optimization for hybrid PV/wind system under various meteorological conditions. *Appl. Energy* **2008**, *85*, 968–987. [CrossRef]
120. Al-Sefri, A.K.; Al-Shaalan, A.M. Availability, Performance and Reliability Evaluation for PV Distributed Generation. *World J. Eng. Technol.* **2019**, *07*, 429–454. [CrossRef]
121. Upadhyay, S.; Sharma, M. Development of hybrid energy system with cycle charging strategy using particle swarm optimization for a remote area in India. *Renew. Energy* **2015**, *77*, 586–598. [CrossRef]

122. Sultan, H.M.; Kuznetsov, O.N.; Menesy, A.S.; Kamel, S. Optimal Configuration of a Grid-Connected Hybrid PV/Wind/Hydro-Pumped Storage Power System Based on a Novel Optimization Algorithm. In Proceedings of the 2020 International Youth Conference on Radio Electronics, Electrical and Power Engineering (REEPE), Moscow, Russia, 12–14 March 2020; pp. 1–7.
123. Arabali, A.; Ghofrani, M.; Etezadi-Amoli, M.; Fadali, M.S. Stochastic Performance Assessment and Sizing for a Hybrid Power System of Solar/Wind/Energy Storage. *IEEE Trans. Sustain. Energy* **2013**, *5*, 363–371. [CrossRef]
124. Nguyen, H.T.; Safder, U.; Nguyen, X.N.; Yoo, C. Multi-objective decision-making and optimal sizing of a hybrid renewable energy system to meet the dynamic energy demands of a wastewater treatment plant. *Energy* **2019**, *191*, 116570. [CrossRef]
125. Mirjalili, S.; Lewis, A. The whale optimization algorithm. *Adv. Eng. Softw.* **2016**, *95*, 51–67. [CrossRef]
126. Nadimi-Shahraki, M.H.; Zamani, H.; Mirjalili, S. Enhanced whale optimization algorithm for medical feature selection: A COVID-19 case study. *Comput. Biol. Med.* **2022**, *148*, 105858. [CrossRef]
127. Suhartini, S.; Lestari, Y.P.; Nurika, I. Estimation of methane and electricity potential from canteen food waste. *IOP Conf. Series: Earth Environ. Sci.* **2019**, *230*, 012075. [CrossRef]
128. Loyyal Website. (December 2021). Luminous Solar . . . —Google Scholar. Available online: https://scholar.google.com/scholar?hl=en&as_sdt=0%2C5&q=Loyyal+Website.+%282021%2C+December%29.+Luminous+Solar+Panel+380Watt+%2F+24Volt+Mono+Perc+%5BCommercial%5D.+Luminous+Solar+Panel+380Watt+%2F+24Volt+Mono+Perc.+https%3A%2F%2Floyyal.in%2Fproduct-details%2Fluminous-solar-panel380watt-24volt-mono-perc+%28Accessed+2022-06-17%29&btnG= (accessed on 22 December 2022).
129. Salama, H.S.; Vokony, I. Voltage and Frequency Control of Balanced/Unbalanced Distribution System Using the SMES System in the Presence of Wind Energy. *Electricity* **2021**, *2*, 205–224. [CrossRef]
130. Jackson, N.D.; Gunda, T.; Gayoso, N.; Desai, J.; Walker, A. Operations, maintenance, and cost considerations for PV+Storage in the United States. United States: N. p., 2022. Web. Available online: https://www.osti.gov/biblio/1899420 (accessed on 24 April 2023).
131. Mongird, K.; Viswanathan, V.V.; Balducci, P.J.; Alam, J.E.; Fotedar, V.; Koritarov, V.S.; Hadjerioua, B. *Energy Storage Technology and Cost Characterization Report*; Pacific Northwest National Lab.: Richland, WA, USA, 2019. [CrossRef]
132. Schröder, A.; Kunz, F.; Meiss, J.; Mendelevitch, R.; Von Hirschhausen, C. *Current and Prospective Costs of Electricity Generation until 2050*; DIW Data Documentation; DIW Berlin, German Institute for Economic Research: Berlin, Germany, 2013.
133. Solar Inverter Costs and How to Choose the Right One. Understand Solar. 23 February 2017. Available online: https://understandsolar.com/solar-inverter-costs/ (accessed on 24 November 2022).
134. Bhattacharjee, S.; Acharya, S. PV–wind hybrid power option for a low wind topography. *Energy Convers. Manag.* **2015**, *89*, 942–954. [CrossRef]
135. Li, C.; Zhang, L.; Qiu, F.; Fu, R. Optimization and enviro-economic assessment of hybrid sustainable energy systems: The case study of a photovoltaic/biogas/diesel/battery system in Xuzhou, China. *Energy Strat. Rev.* **2022**, *41*, 100852. [CrossRef]
136. Mwakitalima, I.J.; Rizwan, M.; Kumar, N. Integrating Solar Photovoltaic Power Source and Biogas Energy-Based System for Increasing Access to Electricity in Rural Areas of Tanzania. *Int. J. Photoenergy* **2023**, *2023*, e7950699. [CrossRef]